CN 53-1040/Q ISSN 0254-5853
CODEN: DOYADI

ZOOLOGICAL RESEARCH

VOLUME 34 ISSUE E3
JUNE 2013

Science Press

ZOOLOGICAL RESEARCH

Volume 34, Issue E3 June 2013

CONTENTS

Articles

Smallest bitter taste receptor (T2Rs) gene repertoire in carnivores

..... *Ling-Ling HU, Peng SHI* (E75)

Maternal-effect Floped gene is essential for the derivation of embryonic stem cells in mice

..... *Bo ZHAO, Yi-Xian CUN, Xie-Chao HE, Ping ZHENG* (E82)

Pilot study on binding of bovine salivary proteins to grit silicates and plant phytoliths

..... *Marcus Mau, Thomas M. KAISER, Karl-Heinz SÜDEKUM* (E87)

Cytotoxicity and genome-wide microarray analysis of intestinal smooth muscle cells in response to hexavalent chromium induction

... *Li-Fang JI, Yuan-Yuan WANG, Zi-Dong ZHANG, Yi-Meng YUAN, Yi-Rui HU, Yang-Feng WEI, Jian NI* (E93)

Adaptation to visual stimulation modifies the burst firing property of V1 neurons

..... *Rui-Long LIU, Ke WANG, Jian-Jun MENG, Tian-Miao HUA, Zhen LIANG, Min-Min XI* (E101)

Cover image: Chinese Bulbul, *Pycnonotus sinensis.* Photo by Zong-Yong FAN

Smallest bitter taste receptor (T2Rs) gene repertoire in carnivores

Ling-Ling HU[1,2], Peng SHI[1,*]

1. *State Key Laboratory of Genetic Resources and Evolution*, *Kunming Institute of Zoology*, *Chinese Academy of Sciences*, *Kunming* 650223, *China*;
2. *University of Chinese Academy of Sciences*, *Beijing* 100049, *China*

Abstract: Bitter taste reception is presumably associated with dietary selection, preventing animals from ingesting potentially harmful compounds. Accordingly, carnivores, who encounter these toxic substances less often, should have fewer genes associated with bitter taste reception compared with herbivores and omnivores. To investigate the genetic basis of bitter taste reception, we confirmed bitter taste receptor (T2R) genes previously found in the genome sequences of two herbivores (cow and horse), two omnivores (mouse and rat) and one carnivore (dog). We also identified, for the first time, the T2R repertoire from the genome of other four carnivore species (ferret, giant panda, polar bear and cat) and detected 17−20 bitter receptor genes from the five carnivore genomes, including 12−16 intact genes, 0−1 partial but putatively functional genes, and 3−8 pseudogenes. Both the intact T2R genes and the total T2R gene number among carnivores were the smallest among the tested species, supporting earlier speculations that carnivores have fewer T2R genes, herbivores an intermediate number, and omnivores the largest T2R gene repertoire. To further explain the genetic basis for this disparity, we constructed a phylogenetic tree, which showed most of the T2R genes from the five carnivores were one-to-one orthologs across the tree, suggesting that carnivore T2Rs were conserved among mammals. Similarly, the small carnivore T2R family size was likely due to rare duplication events. Collectively, these results strengthen arguments for the connection between T2R gene family size, diet and habit.

Keywords: T2R; Bitter taste; Carnivores; Duplication

Bitter taste perception is important for the survival of animals in the wild. In nature, a variety of toxic substances have a bitter taste. Given that bitter perception has been shown to induce animals to display aversion behavior (Garcia & Hankins, 1975; Glendinning, 1994), perception of this taste has potentially evolved as a defense mechanism against ingesting toxic compounds. A decade ago, two groups independently identified a novel family of seven-transmembrane G protein-coupled receptors (GPCRs) as candidate bitter taste receptors (T2Rs) responsible for detection of bitter tastes (Adler et al, 2000; Chandrashekar et al, 2000). The coding regions of T2R genes are ~900 bp long and intronless. Subsequent studies expanded these findings and showed that bitter tastants bind to T2Rs and trigger the bitter taste perception signal transduction pathway (Behrens et al, 2007; Behrens & Meyerhof, 2006, 2009; Chandrashekar et al, 2006; Mueller et al, 2005).

The macroevolution of T2Rs has been well elaborated among several vertebrates, featured by the dynamic change of gene birth and death (Dong et al, 2009; Go, 2006; Go et al, 2005; Shi & Zhang, 2006; Shi et al, 2003). Interestingly, there are ~20 T2R genes in the carnivorous dog (*Canis familiaris*), which is the smallest known T2R gene family in terrestrial mammals discovered to date, with the exception of the dolphin (Jiang et al, 2012). It has been hypothesized that T2R family size in carnivores is smallest, while herbivores possess an intermediate size and omnivores possess the largest, with gene family size related to the amount of bitter toxic compounds they encounter (Shi & Zhang, 2006). To test the accuracy of this hypothesis, we analyzed several carnivore species to accurately investigate the evolutionary pattern of the T2R gene family among the carnivore lineage.

Received: 19 March 2013; Accepted: 10 April 2013
Foundation items: This work was supported by the Key Project (30930015) and General Project (31271329) from National Natural Science Foundation of China
* Corresponding author, E-mail: ship@mail.kiz.ac.cn

The mammalian order Carnivora includes ten families divided into two monophyletic super-families, Caniformia and Feliformia (Yu et al, 2004), which each consist of five families. In the present study, we included five carnivore species from both super-families: the domestic dog, giant panda, domestic ferret, polar bear and domestic cat. Domestic dogs are primarily omnivorous, including both animal and plant foods in their diet (Bhagat, 2002). Giant pandas (*Ailuropoda melanoleuca*) are primarily herbivores, but also include animal foods in their diets (Bies, 2002). The domestic ferret (*Mustela putorius furo*), polar bear (*Ursus maritimus*), and domestic cat (*Felis catus*) are all carnivores with primary diets consisting of terrestrial vertebrates (Anna Toenjes, 2011; Duda, 2003; Gunderson, 2009). The easy availability of the giant panda, domestic ferret, domestic cat, and polar bear genome sequences provides an opportunity to identify the intact carnivorous T2R repertoire, shedding light on the evolutionary mechanism of bitter tastes and the evolutionary adaptations necessary for carnivore survival. To this end, we first identified the T2R genes from these five carnivores and then chose another five mammalian herbivores and omnivores—cow, horse, mouse, rat and human—with different dietary preferences, to compare their T2R genes with those of carnivores in a phylogenetic analysis.

MATERIALS AND METHODS

Data

The genome version for each species was as follows: domestic cat (Felis-catus-6.2, Sep 2011), domestic dog (CanFam 3.1, Sep 2011), giant panda (ailMel1, Jul 2009), domestic ferret (MusPutFur 1.0, Jun 2011), polar bear (BGI-Shenzhen, 2010), cow (UMD 3.1, Nov 2009), horse (EquCab2, Sep 2007), mouse (NCBI 37, April 2007) and rat (RGSC 3.4, Dec 2004).

Detection of T2R genes

Beginning with the human T2R protein sequences reported in our previous paper (Shi & Zhang, 2006), TblastN (Altschul et al, 1997) was used to obtain corresponding T2R sequences from each candidate genome using an E-value less than le-5. All obtained sequences were used to blast the NR database, with the sequence discarded when the best hit was not T2R. To further confirm the results, a tree for all T2R sequences was constructed via the neighbor-joining method, using V1R sequences as the out group. When the T2R sequence was not clustered with candidate T2R genes but was clustered outside of the out-group V1R sequences, the sequence was discarded. We predicted the ORFs for the remaining sequences, and when an ORF was found longer than 800 bp, we assumed it to be an intact T2R gene. If there was a stop codon, we then defined it as a pseudogene. When an ORF was found to be less than 800 bp in length, we assumed it to be a partial gene.

Phylogenetic tree analysis

The translated amino acid sequences of T2R genes in human, mouse, rat, cow, horse, dog, ferret, giant panda, polar bear and cat were aligned using ClustalW (Thompson et al, 1994) with default parameters. The phylogenetic tree was constructed in Mega5 (Tamura et al, 2011) using the neighbor-joining method (Saitou & Nei, 1987) with protein Poisson correction distances (Masatoshi & Sudhir, 2000). The bootstrap values of the tree were evaluated with 1,000 replications (Felsenstein, 1985). The nucleotide sequences of eight dog and polar bear non-functional T2R genes along with eight intact T2R genes were aligned by ClustalW with default parameters. The phylogenetic tree was constructed with Mega5 using the neighbor-joining method with p-distances. Two cow V1R genes were used as an out group.

RESULTS AND DISCUSSION

Carnivore T2R gene repertoires

To characterize the T2R gene repertoire in carnivores, we searched genome sequences from the five selected carnivore species—dog, ferret, giant panda, polar bear and cat—with previously reported human T2R genes as queries. There were three kinds of newly identified genes: intact genes (full-length ORF); putative genes (partial sequences with undisruptive ORF due to incomplete genome sequences); and pseudogenes (sequences with premature stop codons). We ultimately detected the T2R repertoires of the five carnivores, consisting of 12−16 intact genes, 0−1 partial genes, and 3−8 pseudogenes in each species (Table 1). The average fraction of pseudogenes in the five carnivore genome sequences was 27%. All amino acid sequences of intact T2R genes from dog, ferret, giant panda, polar bear, and cat are available in the supplementary data set. The average number of T2R genes among carnivores was 19.4, including 14 intact T2R genes (Table 1).

We chose five other mammals with different dietary preferences to compare their T2R genes with those of the carnivores. The analysis of human, mouse, rat, and cow were performed previously by Shi & Zhang (2006) and Dong et al (2009), but were updated in the present study with high-coverage genomes, with 42, 41, 29 and 45 total T2R genes identified among mouse, rat, cow and horse genomes, respectively (Table 1). Our results were almost identical to those previously reported, with the slight differences likely attributable to different calculation methods. The average numbers of T2R genes detected in genomes of herbivores and omnivores were

Table 1 Number of genes and pseudogenes in vertebrate T2R gene family

Species	Number of Genes				Proportion of Pseudogenes (%)
	Functional	Putatively Functional	Pseudo-genes	Total	
Human[1]	25	1	10	36	28
Mouse[1]	36	0	6	42	14
Rat[1]	36	0	5	41	12
Cow[2]	22	0	6	29	21
Horse[2]	22	1	22	45	49
Dog[3]	16	1	3	20	15
Giant Panda[3]	16	0	4	20	20
Polar Bear[3]	14	0	6	20	30
Ferret[3]	12	0	5	17	29
Cat[3]	12	0	8	20	40
Omnivores-3-Ave[4]	32.3	0.3	7.0	39.7	18
Herbivores-2-Ave	22.0	0.5	14.0	37.0	35
Carnivores-5-Ave	14	0.2	5.2	19.4	27

1:Omnivore; 2:Herbivore; 3:Carnivore; 4:Ave: average

37.0 and 39.7, respectively, (Table 1) and both were higher than that of carnivores. A similar pattern was found in the average number of intact T2R genes.

Bitter compounds are more common in plant than in animal tissue, and as such herbivores are expected to encounter more bitter substances than carnivores (Glendinning, 1994). As expected, the average number of total T2R among the five carnivores (19.4) was smaller than that present in both the herbivores and omnivores (Table 1). This was consistent with our hypothesis that carnivore species (including dogs) should have smaller T2R gene repertoires, on average, compared with herbivores or omnivores. This assumption was further supported by the lower average number of intact T2Rs found in carnivores (14) than in the two herbivore (22) and three omnivore (32.3) species. The smaller number of intact carnivore T2Rs was unsurprising, given their dietary habit adaptations that tend to involve fewer foods with bitter tastants compared with the diets of herbivores and omnivores. Subsequently, as omnivores encounter more bitter tastants than do herbivores (Shi & Zhang, 2006), omnivores should—as we observed—have more intact T2Rs and a larger entire T2R gene family than herbivores.

However, mismatches do exist between feeding ecology and taste receptor evolution (Zhao & Zhang, 2012). For example, the loss of T1R2 in vampire bats may be related to the narrowness of their diet rather than specific diet. Bats with different feeding habits also have pseudogenization or loss of T1R1. However, we are not able to extend this rule in vertebrates. For example, chickens only harbor three T2Rs (Shi & Zhang, 2006) although it is a herbivore and insectivore (Gautier, 2002).

Independent loss of carnivore one-to-one T2R genes

We conducted a phylogenetic analysis based on the alignment of nine intact genes from the five carnivores and the corresponding functional genes from human, mouse, rat, cow and horse. Pseudogene sequences were excluded from analysis. The resulting phylogenetic tree illustrated how the T2R genes of the five carnivores were grouped into one-to-one orthologs and multiple-to-multiple orthologs, consistent with our previous conclusion that T2R genes among humans and mice were grouped into one-to-one and multiple-to-multiple orthologs (Shi et al, 2003).

Among carnivore T2R intact genes, we detected five strict one-to-one orthologs due to frequent gene birth/death in the five carnivores, a main feature of T2R genes among vertebrates (Dong et al, 2009; Go et al, 2005; Shi & Zhang, 2006; Shi et al, 2003). These five strict one-to-one orthologs were separated with the criteria that each gene had one ortholog sequence in each of the five carnivores. For example, the one-to-one ortholog gene tree for the dogT2R1-ortholog cluster (Figure 1) was consistent with the species tree. The other four strict one-to-one orthologs are shown in Figure S1. The strict one-to-one ortholog T2R genes were the most conserved T2R genes among all tested carnivore animals, compared with other T2R orthologs, suggesting that these were crucial for the survival of carnivores, perhaps even for mammals in general (Go et al, 2005; Shi et al, 2003).

Except for the strict one-to-one orthologs present in all five carnivores, there were nine one-to-one orthologs

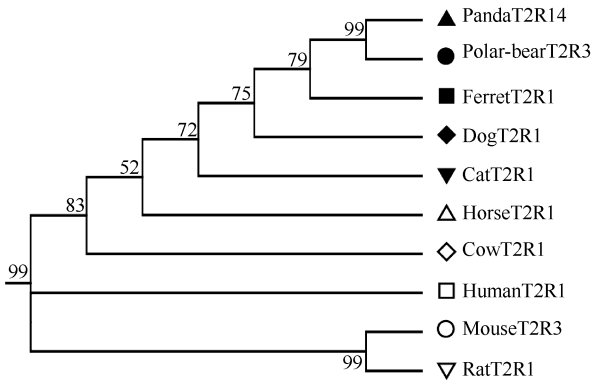

Figure 1 Sub-tree of one strict one-to-one T2R orthologs among ten mammal species

The tree was reconstructed using the neighbour-joining method with protein Poisson distance. Bootstrap values greater than 50% are shown on interior branches. Two V1R genes were used as the out group (not shown).

lost in one or more of the carnivore species. To exclude low quality genome sequences, we used the intact genes as queries to blast each carnivore genome sequences that had lost the ortholog T2R gene and found the corresponding lost T2R pseudogene. We then used the pseudogene to re-blast the query T2R genome to ensure the best hit was the queried T2R. If a species lost one intact T2R gene, we found the lost pseudogene in that genome sequence due to the small evolutionary scale among carnivores. As expected, we searched the candidate genome sequences for the lost intact T2R gene and found each lost pseudo T2R gene for each carnivore, with the exception of the ferret due to low coverage genome quality. For example, for the dogT2R3-ortholog cluster (Figure 2), only one carnivore (polar bear) among the ten species lost this gene. For the dogT2R13-ortholog cluster, three carnivores (cat, ferret and polar bear) lost these genes, along with the horse.

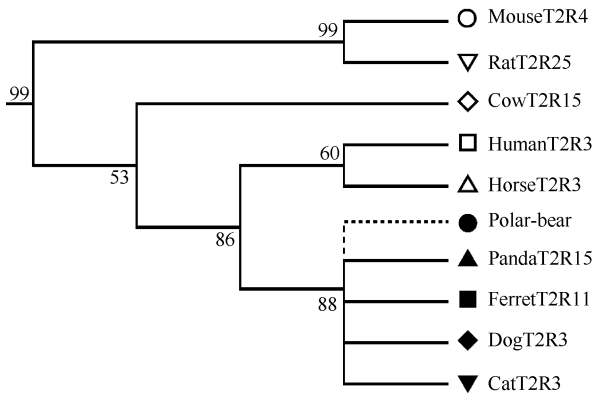

Figure 2 Sub-tree of one-to-one T2R orthologs for the ten species

The tree was reconstructed by the neighbour-joining method with protein Poisson distance. Bootstrap values higher than 50% are shown on interior branches. Two V1R genes were used as the out group (not shown).

Overall, nine one-to-one ortholog genes were lost in different combinations among the different carnivore species. Interestingly, the loss of these particular T2R genes did not occur in the ancestor of the carnivore super-families, Caniformia and Feliformia. This loss of one-to-one ortholog was not lineage-specific, suggesting that the loss of the T2R intact genes among carnivores was species-independent. These incomplete one-to-one ortholog genes showed that these genes were lost randomly in different carnivore species, indicating that the functional T2R genes were important for some species but relaxed in others, likely due to the specific environment in which each species evolved to inhabit.

Rare duplication events among carnivore T2R genes

There were three gene clusters with only one ortholog gene in carnivores, which were duplicated in some non-carnivore species. This kind of T2R genes did not expand in any carnivores and demonstrated a high degree of conservation among these species. For example, in the dogT2R10-ortholog cluster, carnivores had only one copy while mice and rats had five copies. Such an expansion is part of the reason carnivores have such a small T2R family. Conservation of this kind of carnivore T2R gene is likely to maintain the important role they play in the life of carnivores and the increased T2R orthologs among non-carnivore species associated with bitter tastants emerging in their foods compared with carnivore foods. The only exception to this trend was a gene duplicated in cats, giant pandas and ferrets, as well as in all five of the non-carnivore species we investigated. Even for these three carnivores, there were only two copies of the duplicated gene, but in horses and cows there were three and in humans up to eight, which may be responsible for the detection of human-specific tastants (Shi et al, 2003). This similar lack of expansion further explained why carnivores harbored a small T2R family. We considered that after the initial duplication event of T2Rs among carnivores, it did not continue further; but the duplication event continued in non-carnivores after its initial occurrence.

Our results suggested that gene duplication events were virtually non-existent in carnivores. Even though duplication occurred in ferrets, cats and pandas, it did not occur in either dogs or polar bears due to the detection of only one copy of this gene in these two species. The most likely explanation was that one copy was lost independently in both species. To test this possibility, we used all dog and polar bear non-intact T2Rs and all ortholog genes in this duplicated cluster to reconstruct the gene tree in MEGA 5.0. The lost copy of the duplicated cluster in dogs and polar bears was dogps4 and polar bear pseudo3 (Figure 3). This result verified our assumption that both the dog and polar bear each lost one copy of the duplicated gene independently. The pseudogenization of the lost copy of this cluster in dogs and polar bears suggested that the function of this gene was no longer needed or was replaced by other T2R genes as a result of diet and habit adaptation. Further research and comparisons may yield a more complete answer to these types of specific genetic adaptations to dietary needs and to the environment.

The remaining T2R gene clusters were species-specific duplicated genes, most of which were rodents and human specific duplicated genes (Conte et al, 2003; Shi et al, 2003). For this kind of T2R genes, carnivores did not possess any orthologs, though some non-carnivores gained some T2R genes. For example, for this kind of T2R genes, mice and rats gained 16 and 17 T2R genes, respectively (Figure 4), which increased the total number of intact T2R family sizes for those species. For the other three non-carnivores, each gained 3 T2R genes in a similar manner. This increase was further reason for

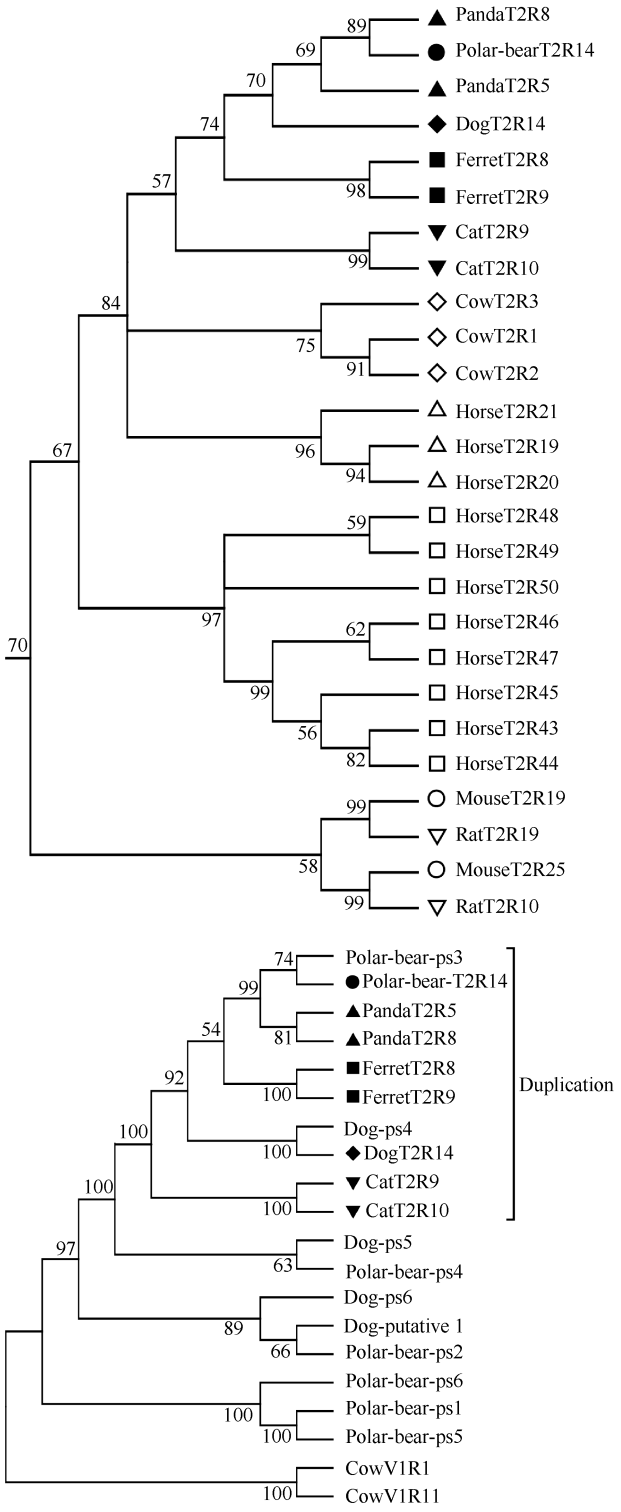

Figure 3 Sub-tree of T2R duplication orthologs for the ten species (3a) and five carnivores (3b)

The tree was reconstructed by the neighbour-joining method with protein Poisson distance (3a) and p-distance (3b). Bootstrap values higher than 50% are shown on interior branches. Two V1R genes were used as the out group.

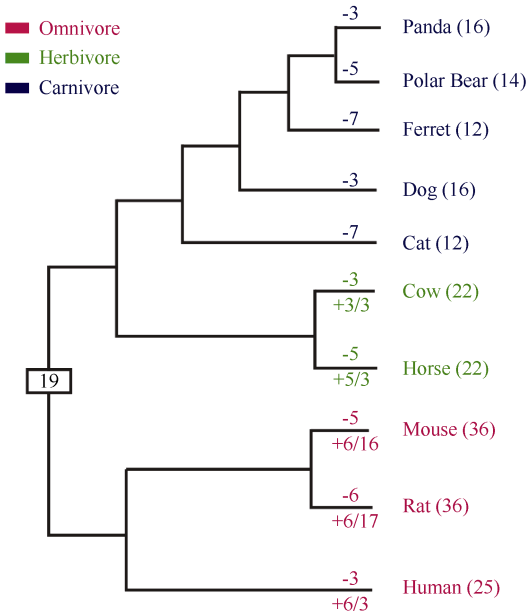

Figure 4 Evolutionary changes in number of intact T2R genes among mammals

Red, green and blue characters stand for omnivore, herbivore and carnivore, respectively. Numbers in rectangle represent the numbers of functional T2R genes in the extant or ancestral species. Numbers with minus and plus signs indicate the numbers of gene losses and gains, respectively, for each branch. Numbers before the slash indicate numbers of carnivore-ortholog gene gains, while those numbers after the slash indicate numbers of non-carnivore-ortholog gene gains.

the relatively small size of the T2R family among carnivores, as carnivores simply did not have orthologs for the genes among non-carnivores. As they do not encounter as many bitter and potentially toxic substances as omnivores or herbivores, carnivores simply do not need to develop sensitivities to such substances. In this scenario, T2R genes likely correspond to species-specific food habits and could be regarded as a molecular adaptation marker to the environment and diet of a specific species.

In short, our findings confirmed that carnivorous mammals, in general, had the smallest T2R family among the three kinds of mammals (carnivores, herbivores and omnivores), which was likely a result of adaptation to the environment. This difference in size was attributable to the fact that a vast majority of carnivore T2Rs were one-to-one orthologs. Even for these conserved T2R genes, some carnivores lost a gene. Overall, carnivores lost 3-7 intact T2R genes (Figure 4), while non-carnivores lost 3-6 intact T2R genes (Figure 4). Both carnivores and non-carnivores lost a similar number of one-to-one T2R ortholog genes. Nevertheless, duplication events occurred only once for one gene cluster in carnivores, while duplication events occurred more than once among non-carnivores. For this category

of T2R genes, which had orthologs in some carnivores, non-carnivores gained 3-6 intact T2R genes (Figure 4). The expanded T2R genes were species-specific gene duplicated genes, especially those in mice and rats, which did not have ortholog genes in any of the five carnivores. The non-carnivore species gained 3-17 intact T2R genes (Figure 4) through this kind of gene duplication. In fact, the five carnivores gained no intact T2R genes, while non-carnivores did. Overall, the small size of the carnivore T2R gene family was due to the relative rarity of gene duplication events in carnivores, while for non-carnivores gene duplication events were the main route for the expanded T2R gene family size.

References

Adler E, Hoon MA, Mueller KL, Chandrashekar J, Ryba NJP, Zuker CS. 2000. A novel family of mammalian taste receptors. *Cell,* **100**(6): 693-702.

Altschul SF, Madden TL, Schaffer AA, Zhang JH, Zhang Z, Miller W, Lipman DJ. 1997. Gapped BLAST and PSI-BLAST: a new generation of protein database search programs. *Nucleic Acids Research,* **25**(17): 3389-3402.

Anna Toenjes N. 2011. "Felis catus" (On-line), Animal Diversity Web. Accessed April 09, 2013 at http://animaldiversity.ummz.umich.edu/accounts/Felis_catus/.

Behrens M, Meyerhof W. 2006. Bitter taste receptors and human bitter taste perception. *Cellular and Molecular Life Sciences,* **63**(13): 1501-1509.

Behrens M, Foerster S, Staehler F, Raguse JD, Meyerhof W. 2007. Gustatory expression pattern of the human TAS2R bitter receptor gene family reveals a heterogenous population of bitter responsive taste receptor cells. *Journal of Neuroscience,* **27**(46): 12630-12640.

Behrens M, Meyerhof W. 2009. Mammalian bitter taste perception. *In:* Korsching S, Meyerhof W. Chemosensory Systems in Mammals, Fishes, and Insects. Berlin Heidelberg: Springer, **47**: 77-96.

Bhagat S. 2002. "Canis lupus familiaris" (On-line), Animal Diversity Web. Accessed April 09, 2013 at http://animaldiversity.ummz.umich.edu/accounts/Canis_lupus_familiaris/.

Bies L. 2002. "Ailuropoda melanoleuca" (On-line), Animal Diversity Web. Accessed April 09, 2013 at http://animaldiversity.ummz.umich.edu/accounts/Ailuropoda_melanoleuca/.

Chandrashekar J, Mueller KL, Hoon MA, Adler E, Feng LX, Guo W, Zuker CS, Ryba NJP. 2000. T2Rs function as bitter taste receptors. *Cell,* **100**(6): 703-711.

Chandrashekar J, Hoon MA, Ryba NJP, Zuker CS. 2006. The receptors and cells for mammalian taste. *Nature,* **444**(7117): 288-294.

Conte C, Ebeling M, Marcuz A, Nef P, Andres-Barquin PJ. 2003. Evolutionary relationships of the Tas2r receptor gene families in mouse and human. *Physiological Genomics,* **14**(1): 73-82.

Dong D, Jones G, Zhang SY. 2009. Dynamic evolution of bitter taste receptor genes in vertebrates. *BMC Evolutionary Biology,* **9**(1): 12.

Duda J. 2003. "Mustela putorius furo" (On-line), Animal Diversity Web. Accessed April 09, 2013 at http://animaldiversity.ummz.umich.edu/accounts/Mustela_putorius_furo/.

Felsenstein J. 1985. Confidence-limits on phylogenies: an approach using the bootstrap. *Evolution,* **39**(4): 783-791.

Garcia J, Hankins WG. 1975. The evolution of bitter and the acquisition of toxiphobia. In: Denton DA, Coghlan JP. Olfaction and Taste V. Proceedings of the 5th International Symposium in Melbourne, Australia. New York: Academic Press, 39-45.

Gautier Z. 2002. "Gallus gallus" (On-line), Animal Diversity Web. Accessed April 09, 2013 at http://animaldiversity.ummz.umich.edu/accounts/Gallus_gallus/.

Glendinning JI. 1994. Is the bitter rejection response always adaptive? *Physiology & Behavior,* **56**(6): 1217-1227.

Go Y, Satta Y, Takenaka O, Takahata N. 2005. Lineage-specific loss of function of bitter taste receptor genes in humans and nonhuman primates. *Genetics,* **170**(1): 313-326.

Go Y. 2006. Proceedings of the SMBE Tri-National Young Investigators' Workshop 2005. Lineage-specific expansions and contractions of the bitter taste receptor gene repertoire in vertebrates. *Molecular Biology and Evolution,* **23**(5): 964-972.

Gunderson A. 2009. "Ursus maritimus" (On-line), Animal Diversity Web. Accessed April 09, 2013 at http://animaldiversity.ummz.umich.edu/accounts/Ursus_maritimus/.

Jiang PH, Josue J, Li X, Glaser D, Li WH, Brand JG, Margolskee RF, Reed DR, Beauchamp GK. 2012. Major taste loss in carnivorous mammals. *Proceedings of the National Academy of the Sciences of the United States of America,* **109**(13): 4956-4961.

Masatoshi N, Sudhir K. 2000. Molecular Evolution and Phylogenetics. New York: Oxford University Press.

Mueller KL, Hoon MA, Erlenbach I, Chandrashekar J, Zuker CS, Ryba NJ. 2005. The receptors and coding logic for bitter taste. *Nature,* **434** (7030): 225-229.

Saitou N, Nei M. 1987. The neighbor-joining method: a new method for reconstructing phylogenetic trees. *Molecular Biology and Evolution,* **4**(4): 406-425.

Shi P, Zhang JZ, Yang H, Zhang YP. 2003. Adaptive diversification of bitter taste receptor genes in Mammalian evolution. *Molecular Biology and Evolution,* **20**(5): 805-814.

Shi P, Zhang J. 2006. Contrasting modes of evolution between vertebrate sweet/umami receptor genes and bitter receptor genes. *Molecular Biology and Evolution,* **23**(2): 292-300.

Tamura K, Peterson D, Peterson N, Stecher G, Nei M, Kumar S. 2011. MEGA5: molecular evolutionary genetics analysis using maximum likelihood, evolutionary distance, and maximum parsimony methods. *Molecular Biology and Evolution,* **28**(10): 2731-2739.

Thompson JD, Higgins DG, Gibson TJ. 1994. Clustal-W: Improving the sensitivity of progressive multiple sequence alignment through sequence weighting, position-specific gap penalties and weight matrix choice. *Nucleic Acids Research,* **22**(22): 4673-4680.

Yu L, Li QW, Ryder OA, Zhang YP. 2004. Phylogenetic relationships within mammalian order Carnivora indicated by sequences of two nuclear DNA genes. *Molecular Phylogenetics and Evolution,* **33**(3): 694-705.

Zhao HB, Zhang JZ. 2012. Mismatches between feeding ecology and taste receptor evolution: an inconvenient truth. *Proceedings of the National Academy of Sciences of the United States of America,* **109**(23): E1464; author reply E1465.

Maternal-effect *Floped* gene is essential for the derivation of embryonic stem cells in mice

Bo ZHAO[1,2,3,*], Yi-Xian CUN[1,2,3], Xie-Chao HE[1,3], Ping ZHENG[1]

1. *State Key Laboratory of Genetic Resources and Evolution, Kunming Institute of Zoology, Chinese Academy of Sciences, Kunming* 650223, *China*;
2. *University of Chinese Academy of Sciences, Beijing* 100049, *China*;
3. *Yunnan Key Laboratory of Animal Reproduction Biology, Kunming Institute of Zoology, Chinese Academy of Sciences, Kunming* 650223, *China*

Abstract: *Floped* (official name *Ooep*) is specifically and abundantly expressed in mouse oocytes and embryonic stem cells (ESCs). Depletion of *Floped* from oocytes leads to early embryonic arrest at the 2-cell stage. Although crucial in cleavage stage development, its roles in early embryos as well as in ESCs remain completely unknown. Here, we compared the efficiency of mouse ESC derivation from inner cell mass (ICM) with and without *Floped* to study its possible roles in mESCs. Derivation rates of mESC from wild-type, heterozygous, and homozygous blastocysts were 33.3%, 21.43%, and 3.85%, respectively, indicating that *Floped-/-* blastocysts had significantly decreased derivation rates. Respective outgrowth appearing rate five days after blastocyst attachment were 83.3%, 85.7%, and 15.4%. Morphologically, the outgrowth of ICM from *Floped-/-* blastocysts appeared severely death three to five days after blastocyst attachment, and the respective derived stem cells showed long-term instability with long-standing epithelial-like colonies. This result suggests a possible role of *Floped* in the course of ICM-ESCs transition.

Keywords: *Floped*; ICM; ESCs

Embryonic stem cells (ESCs) and inner cell mass (ICM) of blastocysts, from which ESCs are derived, possess both similar and dissimilar characteristics (Downing & Battey et al, 2004). The ICM of blastocysts has the potential to develop into a whole embryonic property but loses self-renewal ability. Embryonic stem cells can undergo limitless self-renewal division and maintain the capacity to differentiate into all body cells types (Ying et al, 2008). *In vitro* derivation of ESCs from ICM is a process in which cells switch off the developmental program while retaining pluripotency and gaining self-renewal ability. Although some studies have investigated gene expression changes during derivation, the molecular basis underlying ICM-ESC transition remains unclear.

Floped (factor located in oocytes permitting embryonic development, official name *Ooep*) was originally identified as an oocyte specific gene in mice (Li et al, 2008). The mRNAs of *Floped* are restrictively detected in growing oocytes, but the protein can persist until the blastocyst stage. Genetic ablation of *Floped* from mouse oocytes does not impair the growth, meiotic maturation, or fertilization of the oocytes. Nevertheless, embryos without maternal deposition of the *Floped* protein cannot develop beyond the 2-cell stage when the major zygotic genome activation event occurs (Li et al, 2008). *Floped* is also abundantly expressed in undifferentiated mouse ESCs. Using targeted mutation strategies, a recent study investigated the possible roles of *Floped* in mESCs and found that *Floped* was not necessary for maintaining ESC identity under undifferentiated conditions. However, the absence of *Floped* in mESCs accelerated the differentiation pace when ESCs were induced to undergo differentiation (Miura et al, 2010). Moreover, tracing the derivation of ESCs from ICM by single cell gene expression analysis uncovered a significant increase in mRNA expression of *Floped* during transition, suggesting possible involvement in this reprogramming process (Tang et al,

Received: 08 November 2012; Accepted: 10 January 2013
Foundation items: This work was supported by the Chinese NSFC grant (31171424)
* Corresponding author, E-mail: ytuzhaobo@163.com

2010). Based on these observations, we aimed to investigate the potential roles of *Floped* in the establishment of mESCs from ICM. By utilizing the *Floped* knockout mouse line, our work showed that ICM of *Floped-/-* blastocysts displayed lower potential to transit into ESCs when compared to their wild-type counterparts.

MATERIALS AND METHODS

Ethics statement

All experimental procedures and care of animals were performed according to protocols approved by the Ethics Committee of the Kunming Institute of Zoology, Chinese Academy of Sciences (permit number: SYDW-2006-006).

Feeder cells preparation

Mouse embryonic fibroblasts (MEF) from E14 embryos of CD1 mice were prepared and cultured as previously described (Nagy, 2003). Briefly, MEF were plated in culture dishes precoated with a 0.1% (w/v) solution of gelatin (AMRESCO. 9764-500g) and cultured in DMEM (Gibco; 430-1600) supplemented with 10% newborn calf serum (NCS; Gibco. 16010-159). To prepare the feeder cells in the ESC culture, MEF growing near confluence were treated with mitomycin C (5 μg/mL, Sigma M4287) for 3 hours followed by rinsing five times with Ca^{2+}-, Mg^{2+}-free phosphate buffered saline (PBS). These cells were then trypsinized with 0.05% Trypsin-EDTA (Gibco; 25200-056) and seeded at a density of 5×10^4 cells/cm^2 after washing.

Animals and blastocysts collection

The *Floped-/-* mice were kindly provided by Dr. Lei LI from the Institute of Zoology, Chinese Academy of Sciences. The *Floped+/-* females were mated with *Floped+/-* males at four weeks of age and the mating plug was examined every morning. Females who achieved successful mating were immediately separated from males and blastocysts were collected at E3.5. Morphologically healthy blastocysts were used to derive ESCs. The zonae pellucidae of the blastocysts were removed by incubation with acid Tyrode solution (pH 3; Sigma T1788-100 mL).

Derivation and propagation of ES cells

We used serum-free media supplemented with knockout serum replacement to facilitate the derivation of C57BL/6J mouse ES cell lines (Cheng et al, 2004; Tanimoto et al, 2008) and derive ESCs from blastocysts.

The ES medium was composed of DMEM/F12 supplemented with 20% Knockout Serum Replacement (Gibco; 10828-028), penicillin (100 U/mL)/streptomycin (100 μg/mL) (Gibco; 15140-122), 2 mmol/L of L-glutamine (Sigma; G8540-25 g), 1×MEM Non-Essential Amino Acids Solution (Gibco; 11140-035), 100 μmol/L of beta-mercaptoethanol (Sigma; M7522), and recombinant mouse leukemia inhibitory factor (1 000 U/mL; Chemicon no. ESG1107).

Blastocysts without zona pellucidae were plated on mitomycin C-treated MEFs. Blastocysts were allowed to attach to MEFs and grew without any interference for 48 hours. After five days, the outgrowths were selectively collected and transferred into droplets of 0.05% trypsin-EDTA solution for 1−3 min with a mouth-controlled micropipette (Bryja et al, 2006). Dissociated individual cells and small cell clumps were pipetted directly into a 4-well plate containing new MEFs and ES medium. After continued purification, the putative ES cells were frozen at a concentration of 2×10^6 cells per vial. Cultures were maintained in a humidified incubator at 37 °C, under 5% CO_2 and 95% air.

PCR genotype of the blastocysts

Each blastocyst used for ESC derivation was genotyped by PCR amplification according to previous research (Li et al, 2008). Genomic DNA was extracted from individual blastocysts or its derivatives using a Tianamp Micro DNA Kit according to manufacturer's instructions (TIANGEN BIOTECH; DP316). Primers P1 (5'-CCCTGCTGACAGTGGACTC-3'), P2 (5'-CCAGCCAGTTTTA GCCCTTT-3'), and P3 (5'-TGCGCAACTGTTGGGAAG-3') were used for PCR genotyping.

The PCR conditions consisted of 1 cycle at 95 °C for 3 min; 32 cycles at 94 °C for 30 s, 55 °C for 30 s, 68 °C for 60 s, and a full extension cycle at 72 °C for 7 min. The PCR with three primers produced a 512 bp band (primers P1, P2) in wild-type and an 890 bp band (primers P1, P3) in null and heterozygous mice.

To follow up the ESC lines establishment of three genotypic kinds of *Floped* blastocysts, we collected all derivatives of the blastocysts for respective genome DNA extraction. If one blastocyst did not hatch within 48 hours after seeding, we collected this blastocyst for DNA extraction. As such, derivatives from respective hatched blastocysts were collected regardless of the ES-like cells, peripheral primitive endoderm-like cells, or trophectoderm-derived cells.

Alkaline phosphatase staining

During the log phase, ES cells were fixed by 4% ice-cold paraformaldehyde (PFA) for 1 minute, after which rinsed wells and added enough staining solution (BCIP/NBT Alkaline Phosphatase Color Development Kit; Beyotime C3206) for 15 minutes at room temperature, then count the number of atropurpureus stem cell colonies (AP) versus the number of differentiated colonies (colorless).

Immunocytostaining

Cells were fixed with 4% paraformaldehyde for 30 minutes at room temperature, permeabilized with 0.1% TritonX-100 in PBS for 10 minutes, incubated with PBS containing 1% BSA for 60 minutes to block non-specific reactions, and incubated with anti-Nanog, Oct4, and SSEA-1 antibody (Santa Cruz) overnight at 4 °C. Dilution ratio of the first antibodies was 1:200. After washing with PBS, the cells were incubated with Alexa-Fluor-488-conjugated secondary antibody (Life Technology). Negative controls for fluorophore-conjugated secondary antibody were carried out without primary antibody, and nonspecific binding of secondary antibodies was detected. Fluorescent images were captured using a Leica TCS SP5 confocal microscope system (Leica Microsystems).

Statistical analysis

Data analysis was performed using SPSS 13.0 statistical software. Fisher's exact test was performed. $P<0.05$ was considered statistically significant.

RESULTS

***Floped* for outgrowth formation**

As summarized in Table 1, a total of 15 outgrowths were obtained after five days of culture from 18 wild-type blastocysts (outgrowth rate: 83.33%, 15/18, three females). A similar outgrowth rate was obtained from blastocysts with heterozygous genotype under the same experimental conditions (85.71%, 36/42, three females); in contrast, only 15.38% (4/26, three females) of *Floped-/-* blastocysts demonstrated outgrowth formation.

Table 1 Outgrowth and embryonic stem cell line derivation efficiency from different genotypic blastocysts

Floped	Number of blastocysts used	Number of (%) outgrowths at day 5	Number of ES lines (% blastocyst)	Percentage of ES lines (from outgrowth)
+/+	18	15 (83.33) [a]	6 (33.3) [c]	40 [e]
+/–	42	36 (85.71) [a]	9 (21.43) [c, d]	25 [e]
–/–	26	4 (15.38) [b]	1 (3.85) [d]	25 [e]

Values with different superscripts are significantly different in one column ($P < 0.05$) by Fisher's exact test. Values with same superscripts indicate numbers in the same column are not significantly different ($P > 0.05$).

We found that *Floped-/-* blastocysts could normally attach to feeder cells and grow in the first two days. However, the sizes of the *Floped-/-* outgrowths were smaller than their wild-type or heterozygous counterparts (Figure 1C1, C2). Outgrowths from wide-type and heterozygous blastocysts maintained typical stem-cell like morphology five days after attachment to MEFs, while the majority of *Floped-/-* outgrowths (22/26, 84.6%) started to display signs of death, with ICM derived outgrowth disappearing and only trophectoderm-derived cells left (Table 1; Figure 1C3).

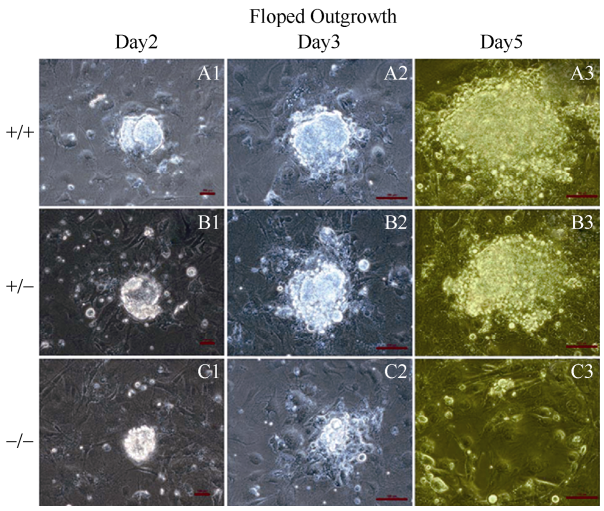

Figure 1 Representative outgrowth morphology from day 2 to day 5 after blastocysts attachment (scale bar=100 μm)

Depletion of *Floped* and derivation of ES cell lines from blastocysts

To establish ESCs from outgrowth, each outgrowth after five days of culturing was manually collected and dispensed into a single cell or small clusters through trypsinization. These cells were cultured and purified continuously for 20−30 days to obtain stable ES cell lines. From this, we obtained six wild-type ESC lines from 15 outgrowths (6/15, 40%), nine ESC lines from *Floped+/-* outgrowths (9/36, 25%), and one ESC line from *Floped-/-* outgrowths (1/4, 25%). From blastocysts, the derivation rates of wild-type, *Floped+/-*, and *Floped-/-* ESC lines were 33.3%, 21.43%, and 3.85%, respectively (Table 1).

It took much longer to purify the *Floped-/-* ESC line than it did to purify the wild-type or heterozygous counterparts. During passage and purification, stable ES cell lines from wide-type and/or heterozygous blastocysts were easily obtained. We purified these cells without the appearance of obvious epidermal-like colonies. In contrast, purification of the *Floped* null ES cell line was very difficult. As shown in Figure 2, epithelial-like colonies appeared at the first passage from outgrowth and continued for two months, even though we collected typical ES-like colonies manually for further culture at every passage. After two months, these epithelial-like colonies disappeared gradually and the stable *Floped* null ES cell line was established.

***Floped* null ES cell characteristics**

Morphology of the ES cell lines is shown in Figure

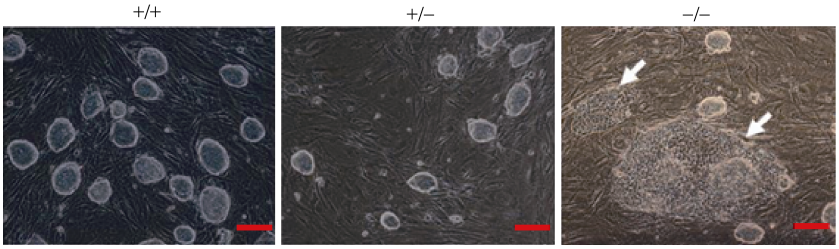

Figure 2 Purification of stem cells after five days of outgrowth

White arrows indicate epithelial-like colonies, scale bar=100 μm.

3A. *Floped* null ES cells, together with wide-type and heterozygous cells, showed typical mouse ES cell morphology, e.g. high ratio of nucleus to cytoplasm and prominent nucleoli, with colonies consisting of small juxtaposed spheroid cells and strong positive staining for alkaline phosphatase (Figure 3A). The ES cells showed high expression of pluripotency markers including Oct4, SSEA-1, and Nanog (Figure 3B-D, respectively). These results indicated that *Floped* was dispensable for ES cell self-renewal after successful derivation from ICM.

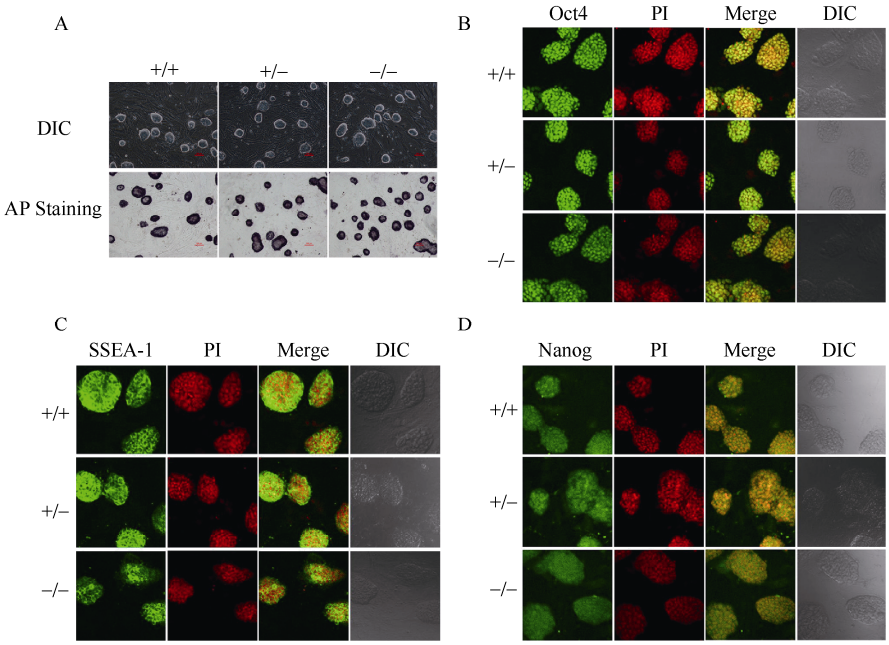

Figure 3 Pluripotency analysis of the ESCs

A) Morphology and alkaline phosphatase activity in ESCs after successful purification; B, C, D) Oct4, SSEA-1, and Nanog immunocytostaining analysis, respectively. scale bar=100 μm.

DISCUSSION

Establishing an ES cell line consists of dynamic molecular changes that accompany cell-fate changes, during which the ICM transform into cells with a capacity for infinite self-renewal while retaining pluripotency (Tang et al, 2010). Cultured ES cells have been assumed to be equivalent, or even identical to cells of the ICM of the blastocyst stage embryo from which they are derived (Reijo Pera et al, 2009). However, no evidence suggests that ICM cells can self-renew extensively. Comparison of global gene expression between individual ICM clusters and human embryonic stem cells indicate that these two cell types are significantly different in regards to gene expression, with less than one half of all genes expressed in both cell types (Reijo Pera et al, 2009). The ICM-ESCs transition is accompanied by complex genomic and epigenetic changes, and further study is required to fully understand this transition. We reported that the maternal effect *Floped* gene had a key function during ICM-ESCs transition, without which the transition rate of success was compromised, but had no influence on ES cell cultivation after successful derivation.

Gene expression data suggests a potential role of *Floped* in ICM-ESCs transition. With Oct4-DPE-GFP transgenic mice, Tang et al (2010) traced the

transcriptional, epigenetic, and miRNA transitions during the ICM-ESCs switching process. In their single cell RNA-seq database, the *Floped* expression counts were 1 352 in ICM, 598 in day 3 outgrowth Oct4 positive cells, 7525 in day 5 outgrowth Oct4 positive cells, and 11259 in ESCs; however, were 72 in day 5 outgrowth Oct4 negative cells. The expression counts of *Floped* decreased from ICM to day 3 outgrowth, but increased sharply from day 3 to day 5 outgrowth, and increased further from day 5 outgrowth to ESCs. These data indicated that *Floped* may have an important role during ESC line derivation from day 3 outgrowth to ESCs. In addition, the 72 *Floped* count on day 5 outgrowth Oct4 negative cells indicated that *Floped* was specifically expressed in pluripotent cells that progress toward ESCs, instead of differential cells. These are in agreement with the RNA-seq counts above.

We found that *Floped* null outgrowths died between days 3 and 5. We concluded, therefore, that *Floped* viably effected outgrowth, with a subsequent increased total cell number resulting from cell culture. This effect is beneficial for the later establishment of a stem-cell line.

Floped was highly expressed in self-renewing ES cells, and its expression was downregulated upon differentiation. The ES cells without *Floped* expression showed no obvious abnormalities in their undifferentiated state (Miura et al, 2010). Our results confirmed that *Floped* null ES cells had typical morphology, with stable passaging. In the process of stem cell purifying, however, many epithelial-like colonies appeared in the *Floped* null line, which suggested these cells were in an unstable state. After a period of continuous culture, the *Floped* null stem cells adapted to the in vitro environment and became stable. These data indicated that *Floped* had a key function during the establishment process of the ES cell lines, but no notable function in maintaining the ES cell self-renewal state after successful purification.

Further study is required to fully understand the molecular mechanisms of *Floped* during ESC derivation, which will increase our knowledge on the molecular changes of this process and accelerate the application of embryonic stem cells.

References

Bryja V, Bonilla S, Čajánek L, Parish CL, Schwartz CM, Luo YQ, Rao MS, Arenas E. 2006. An efficient method for the derivation of mouse embryonic stem cells. *Stem Cells,* **24**(4): 844-849.

Cheng J, Dutra A, Takesono A, Garrett-Beal L, Schwartzberg PL. 2004. Improved generation of C57BL/6J mouse embryonic stem cells in a defined serum-free media. *Genesis,* **39**(2): 100-104.

Downing GJ, Battey JF Jr. 2004. Technical assessment of the first 20 years of research using mouse embryonic stem cell lines. *Stem Cells,* **22**(7): 1168-1180.

Li L, Baibakov B, Dean J. 2008. A subcortical maternal complex essential for preimplantation mouse embryogenesis. *Developmental Cell,* **15**(3): 416-425.

Miura M, Ueda A, Takao Y, Nishimura EK, Koide H, Yokota T. 2010. A stem cell-derived gene (Sddr) negatively regulates differentiation of embryonic stem cells. *International Journal of Developmental Biology,* **54**(1): 33-39.

Nagy A. 2003. Manipulating the Mouse Embryo: A Laboratory Manual. New York: Cold Spring Harbor Laboratory.

Reijo Pera RA, de Jonge C, Bossert N, Yao M, Yang JYH, Asadi NB, Wong W, Wong C, Firpo MT. 2009. Gene expression profiles of human inner cell mass cells and embryonic stem cells. *Differentiation,* **78**(1): 18-23.

Tang CH, Barbacioru C, Bao SQ, Lee C, Nordman E, Wang XH, Lao KQ, Surani MA. 2010. Tracing the derivation of embryonic stem cells from the inner cell mass by single-cell RNA-Seq analysis. *Cell Stem Cell,* **6**(5): 468-478.

Tanimoto Y, Iijima S, Hasegawa Y, Suzuki Y, Daitoku Y, Mizuno Y, Ishige T, Kudo T, Takahashi S, Kunita S, Sugiyama F, Yagami K. 2008. Embryonic stem cells derived from C57BL/6J and C57BL/6N mice. *Comparative Medicine,* **58**(4): 347-352.

Ying QL, Wray J, Nichols J, Batlle-Morera L, Doble B, Woodgett J, Cohen P, Smith A. 2008. The ground state of embryonic stem cell self-renewal. *Nature,* **453**(7194): 519-523.

Pilot study on binding of bovine salivary proteins to grit silicates and plant phytoliths

Marcus MAU[1,3,*], Thomas M. KAISER[2], Karl-Heinz SÜDEKUM[3]

1. *Saliva Research Unit, Dental Institute, King's College London, London, UK*;
2. *Zoological Institute and Museum, University of Hamburg, Hamburg, Germany;*
3. *Institute of Animal Science, University of Bonn, Bonn, Germany*

Abstract: Mostly fed with grass in fresh or conserved form, cattle and other livestock have to cope with silicate defence bodies from plants (phytoliths) and environmental silicates (grit), which abrade tooth enamel and could additionally interact with various salivary proteins. To detect potential candidates for silicate-binding proteins, bovine whole saliva was incubated with grass-derived phytoliths and silicates. Interactions of salivary proteins with pulverized bovine dental enamel and dentine were additionally analysed. After intense washing, the powder fractions were loaded onto 1D-polyacrylamide gels, most prominent adhesive protein bands were cut out and proteins were identified by mass spectrometry within three independent replicates. All materials were mainly bound by bovine odorant-binding protein, bovine salivary protein 30×10^3 and carbonic anhydrase VI. The phytolith/silicate fraction showed additional stronger interaction with haemoglobin β and lactoperoxidase. Conceivably, the binding of these proteins to the surfaces may contribute to biological processes occurring on them.

Keywords: Bovine salivary proteins; Mass spectrometry; Phytoliths; Silicates; Tooth enamel

Grasses highly mineralise parts of their cells and bodies with opaline silicates. These so-called phytoliths are considered to be a mechanical defense against herbivory by abrading mammalian tooth enamel and dentine (Baker et al, 1959; McNaughton & Tarrants, 1983). However, their effectiveness to do so has not been resolved conclusively to date and there are ongoing discussions about the hardness of phytoliths compared to enamel (Sanson et al, 2007). In addition, for decades and also today field studies have indicated that the ingestion of soil might have a greater impact on tooth abrasion in grazing ruminants (Healy & Ludwig, 1965; Healy et al, 1967; Hummel et al, 2011). In fact, excessive dental wear is an important problem especially in sheep production throughout New Zealand. As early as in the 1960's, soil ingestion was believed the main reason for the large distribution of wear in sheep and it was found that the degree of wear directly correlated with the quantity of soil taken in (Healy & Ludwig, 1965; Ludwig et al, 1966; Healy et al, 1967). Interestingly, it could be observed that a reduction in soil intake by providing supplementary feed also reduced the wear caused in sheep (Healy et al, 1967). Moreover, the process of tooth decay in sheep seems to include dissolving processes that are supposedly caused by acids originating from herbs and soil (Michum & Bruere, 1984; Bloxham & Purton, 1991).

To cope with dietary acids and other deterrents in general saliva is saturated with bicarbonate and calcium phosphate and thus secures dental integrity by controlling local pH and tooth remineralisation with the help of various salivary proteins and enzymes (Kaplan & Baum, 1993; Dowd, 1999). Although increased wear and chemically induced tooth decay have been observed in grazing ruminants, none of the studies so far examined the interactions of dietary silicates with salivary proteins with yet unknown consequences on enzyme activities and protein functions.

The present study for the first time sought to show binding of ruminant salivary proteins to dental enamel, dentine and isolated environmental grit/phytoliths.

Received: 07 November 2012; Accepted: 10 January 2013
Foundation items: This research was supported by the German Research Foundation (DFG, SU 124/15-1).
* Corresponding author, E-mail: mmau@itw.uni-bonn.de

Especially phytolith-binding could be a way of how salivary proteins, that are involved in pH and wear control, might be inactivated or functionally inhibited. As a result tooth decay would be observed in grazing livestock, confronted with high-silicate feed.

MATERIAL AND METHODS

Saliva samples

Because of its easiness to collect, saliva of three cows (*Bos primigenius f. taurus*) instead of sheep saliva was obtained from the Leibniz Institute for Farm Animal Biology (FBN) in Dummerstorf, Germany. Natural salivary flow was collected and food particles were subsequently precipitated by centrifugation at 300 r/min for 5 min. Supernatants were harvested and stored in 1.5 ml aliquots at −80 °C until use. Total protein concentrations were determined before freezing against bovine serum albumin standard using the micro bicinchoninic acid method (Kit BCA-1 and B 9643, Sigma-Aldrich, Taufkirchen, Germany).

Phytolith/Silicate preparation

For phytolith extraction from grass/hay pellets a dry ash method was used according to Parr et al (2001) using a muffle oven, 10% HCl and 15% H_2O_2 for washing and the removal of carbonates and organic material. In detail, 1.0 g of dried plant material was ground in a mortar, washed in distilled water and transferred to crucibles. Crucibles were moved to a muffle oven and the plant material was incinerated overnight at 500 °C. After cooling to room temperature, 10 mL of 10% HCl were added and the mixture was incubated at 70 °C for 20 min. After centrifugation (3500 r/min; 5 min) the supernatant was decanted, the pellet washed and immediately 10 mL of H_2O_2 were added to incubate at 70 °C for 20 min. After a second centrifugation step, pellets were washed 2 times with distilled water and phytolith/silicate pellets were air-dried overnight. Isolated materials were weighed separately and related to 1.0 g dry weight to get the percentage of silicates per sample. After that, isolates were pooled and kept in a 1.5 mL reaction tube at −80 °C until further use.

Bovine dental enamel and dentine preparation

Lower bovine jaws of two cows were obtained also from the FBN in Dummerstorf, Germany, and were prepared with minor changes to the method earlier described by Mau et al (2006). The frozen jaws were cut to expose the teeth using a diamond saw. Subsequently, crowns of lower molars m1, m2 and m3 were cut using the same diamond saw, manually freed of connective tissues with the help of a scalpel and stored at −80 °C.

For the experiments teeth were thawed and 4 mm×4 mm×2 mm discs were cut starting at the smooth surface produced by the diamond saw. After washing the discs in distilled water in an ultrasonic bath (Bandelin Sonorex RK 100) for 5 min, enamel and dentine were separated, dried and ground in a mortar. Right after, the resulting powder fractions were sieved using a mesh cascade of 300 μm, 200 μm, 180 μm, 125 μm and 90 μm. The powder <90 μm was weighed and kept in 1.5 ml reaction tubes. After washing five times with distilled water and subsequent centrifugation at 2000 r/min for 10 min, the powders were dried at 37 °C and stored at −80 °C until use.

Incubation experiments and gel electrophoresis

Dental enamel, dentine and phytoliths were thawed and 6 mg of each powder were weighed into individual 1.5 mL reaction tubes. Samples were then added either 200 μL bovine whole saliva or 200 μLof distilled water (negative controls) and incubated at 37 °C for 4 h with constant agitation. This experiment was repeated three times.

After incubation, samples were centrifuged at 2000 r/min for 5 min and supernatants were kept. Powder samples were subsequently washed six times with 200 μL 0.9% NaCl solution and centrifuged at 2000 r/min for 5 min. First, third and sixth washing fractions were collected for gel electrophoresis as a control of washing effectiveness. Finally, powder samples with remaining, bound proteins were added 10 μl reducing loading buffer, heated for 5 min at 95 °C and run on 10% resolving gels in 1D-SDS-PAGE at 125 V for 2 h.

Right after electrophoresis, gels were stained with Coomassie-R250 over night and de-stained for up to 4 h the following day. Stained gels were documented using a standard horizontal scanner and after that bands of interest were cut out and prepared for mass spectrometry (MS).

Mass spectrometry and protein identification

Protein bands bound to enamel, dentine or phytoliths were excised from all three replicates. Gel pieces were subsequently de-stained, and digested with trypsin. In details, bands were de-stained in water and 50% (v/v) acetonitrile and freeze-dried. Gel pieces were rehydrated with digestion buffer (50 mmol/L NH_4HCO_3) containing a 1:20 dilution of trypsin (Promega, Madison, WI, USA) and incubated overnight at 37 °C. Peptides were acidified with formic acid, and loaded via auto-sampling to a C_{18} PepMap100 column (HPLC ultimate 3000; Dionex, Sunnyvale, CA, USA).

Protein identification was done on a MS HCTultra PTM Discovery system (Bruker Daltonics, Billerica, MA, USA). The generated mass spectra were used to search the NCBI protein database with the help of Data Analysis, Version 3.4.192.1 (Bruker Daltonics), and the Mowse MASCOT-software (Matrix-Science, Boston, MA, USA).

Individual thresholds of 95% (P<0.05) for Mowse were considered for confident protein identification.

RESULTS

Phytolith isolation from grass pellets

Acid-insoluble silicates isolated from grass pellets were evaluated by light microscopy and searched for phytolith crystals. The mean abundance of phytoliths/silicates in the grass samples was calculated with 1.2%, which is very similar to the values described for pasture samples given by Healy & Ludwig (1965; Table 1). Phytoliths were mainly bilobate short cell-type (according to international nomenclature; Madella et al, 2005) with a mean diameter of 22.8 μm (Figure 1). Interestingly, in some cases the *in situ* arrangement of phytoliths was still present after incineration and acid solubilisation (Figure 1A, B). The majority of the prepared silicates was much larger than the phytoliths and showed irregular shapes. These silicates are considered to be of anorganic origin, representing dust and grit that is found on grass surfaces. However, the sole use of purified phytoliths was not intended in this study, putting emphasize on the fact that herbivores feeding on grass would have to cope with both grit silicates and biogenic phytoliths in their diets. Lucerne pellets were used as a negative control for phytoliths and showed almost no silicate content (Table 1).

Table 1 Acid-insoluble ash from grass and a grass-grain-mixture contain phytoliths and environmental silicates, which are chewed on by herbivorous animals during grass-eating

Sample	Acid-insoluble silicate fraction in per gram sample (mean±*SD*)	Silicate proportion in %
Grass	0.012±0.0032	1.20
Grass/Grain	0.009±0.0021	0.93
Lucerne	0.00012±0.00022	0.012

Lucerne, which is considered free of phytoliths, served as negative control.

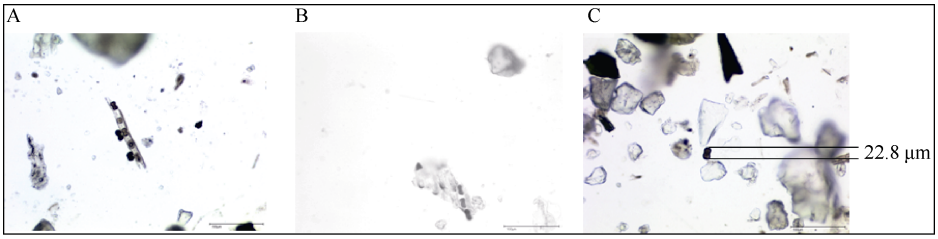

Figure 1 Microscopic evidence for the presence of phytoliths in grass preparations

A, B: showing the characteristic bilobate short cell-form of phytolith; C: a single phytolith in comparison to the irregular appearance of environmental silicates. The mean length of the phytoliths prepared was 22.8 μm. Scale bar=100 μm.

Binding of bovine salivary proteins to enamel, dentine and silicates and their identification by mass spectrometry

Protein concentrations in the three bovine saliva samples were 1.056, 1.126 and 1.050 mg/ml, respectively. After incubation of enamel, dentine and phytolith powders with bovine saliva the six washing fractions contained decreasing protein in accordance to an earlier study by Mau et al (2006). The sixth washing fraction did not contain any protein, which was tested by Coomassie R-250 gel staining (not shown). The powder was then loaded on the gel and bound proteins were electro-eluted and subsequently visualized by Coomassie staining (Figure 2). Silicate, enamel and dentine powders incubated with distilled water served as negative controls to test for proteins originating from the tooth materials. Although enamel and dentine, the latter with its higher content of collagen fibres, showed a high-molecular protein smear at the entrance of the dissolving gel, there were no clearly identifiable protein bands detected in these negative controls (Figure 2).

Bovine odorant-binding protein (OBP), bovine salivary protein 30×10^3 (BSP30) and carbonic anhydrase VI (CA-VI) were the most abundant protein fractions bound to silicates, tooth enamel and dentine, the latter of which is also exposed on the ruminant tooth surface (Figure 2; Table 2). Interestingly, the phytolith/silicate samples additionally interacted with haemoglobin β and lactoperoxidase, two proteins that were only found to bind at a very low extent to the dental materials (Figure 2; Table 2).

DISCUSSIONS

We have identified interactions of bovine salivary proteins with dental materials and food-derived silicates by using a protein binding approach. Adhered salivary proteins belonged to four different functional classes of proteins with putative roles in odorant binding (OBP), oxygen binding (haemoglobin β), pH regulation (CA-IV) and anti-bacterial defence (lactoperoxidase, BSP30). However, we could not identify salivary proteins such as mucins that have been earlier described in playing a potential role in tooth protection against mechanical or

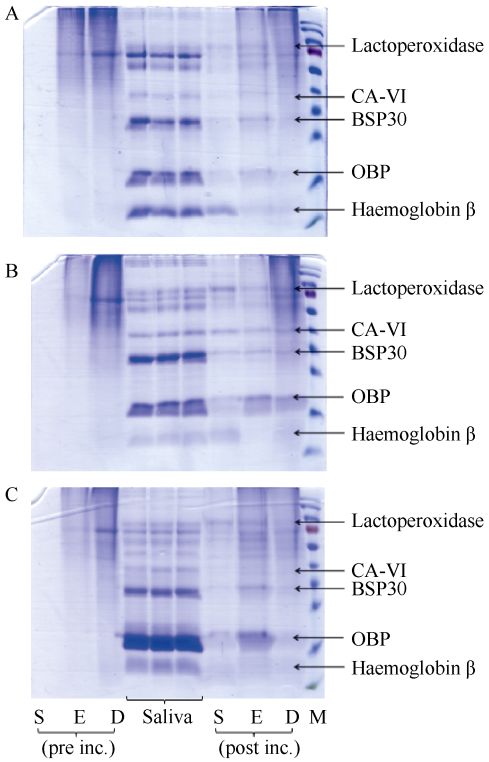

Figure 2 Bovine salivary proteins with binding affinities to silicate (S), enamel (E) and dentine (D) were analysed and identified by 1D SDS-PAGE and MS/MS mass spectrometry using saliva obtained from three different animals (A, B, C).
S: silicate; E: enamel; D: dentine; CA-VI: carbonic anhydrase, VI. BSP30; bovine salivary protein 30×10^3; OBP; odorant-binding protein; M; Fermentas prestained protein standard (SM0671, Fermentas, St. Leon-Rot, Germany).

chemical damage (Tabak, 1995).

The CA-VI, OBP and BSP30 have also been demonstrated in an earlier study to interact with bovine enamel and dentine and therefore this new study supports the former findings (Mau et al, 2006). Additionally CA-VI, OBP, BSP-30 and lactoperoxidase have been identified recently in a first global survey of the bovine salivary proteome (Ang et al, 2011). Although Ang et al (2011) suggested a functional classification of bovine salivary proteins, still little is known about the roles of certain proteins in cattle physiology.

There are indications coming from pigs that the highly abundant salivary OBP primarily acts as a transporter for odorants to their specific receptor sites in the nasal or vomeronasal mucosa (Tegoni et al, 1996; Guiraudie et al, 2003). The latter of which is only accessible due to activated channeling using a duct located between the incisors (Takami, 2002). As the teeth provide a large surface area in the mouth, they are the first oral structures that get into contact with odorants derived e.g. from cow urine during flehmen as it has been proposed earlier for porcine OBP (Guiraudie et al, 2003). Specific binding of odorants by bovine OBP immobilized to the tooth surface may result in a higher local concentration of odorants/pheromones in the mouth by which the chance of recognition in the vomeronasal organ would be increased (Mau et al, 2006).

Haemoglobin is another protein that usually interacts with silicates (Everest et al, 2006). Interestingly, binding to silica has stabilizing effects on haemoglobin against the influence of high temperature and harsh salt conditions and thereby could guarantee the activity and function of the molecule (Urabe et al, 2007). However, the origin of the protein in bovine saliva is unknown and the contamination of saliva with blood during sampling cannot be totally excluded.

The two carbonic anhydrases (CA-II and CA-VI) present in ruminant saliva might work together in providing bicarbonate that is needed to buffer the salivary pH and the neutral to slightly acidic milieu in the rumen (Asari et al, 1989, 2000; Mau et al, 2010). However, recent research on protein adsorption onto silica particles suggests that carbonic anhydrases, when binding to silica surfaces, undergo conformational changes able to alter the enzymatic activity and stability (Karlsson et al, 2000; Lundqvist et al, 2004). For example for human carbonic anhydrase II it was demonstrated that the enzyme first rapidly binds to the particle surface. Then it undergoes stepwise conformational changes causing the active site to unfold, before the rest of the tertiary enzyme structure breaks, leading to an inactive enzyme (Karlsson et al, 2000). Considering that similar processes occur during the interaction of salivary CA with dietary silicates and grit, this could explain the observed acid-induced tooth decay in sheep after herbage and soil consumption due to impaired oral pH control. However, to test this hypothesis, further functional work is necessary on the interaction of salivary CA and silicates in grazing farm animals.

Silica-binding of lactoperoxidase was earlier described to probably occur from electrostatic and/or hydrophobic interactions (Svendsen et al, 2006). As bacteria and especially soil bacteria like *Bacillus subtilis* bind to silicates with high affinity (Mera & Beveridge, 1993; Grantham & Dove, 1996), it is assumed that the preferential binding of lactoperoxidase to environmentally derived silicates (phytoliths and grit) might be a first defence line against invading pathogens. Thereby the local concentration of this antimicrobial enzyme is increased in the mouth right at the reactive surface. Lactoperoxidase might be supported in its antibacterial defence activity by the highly abundant BSP30 that has been suggested to play a role in microbial-host interaction (Haigh et al, 2008; Wheeler et al, 2011) and could act as a modulator of rumen ecology (Wheeler et al, 2011).

In conclusion, we showed for the first time that bovine salivary proteins interact besides dental materials

Table 2 Protein identification results from *Bos primigenius f. taurus* for salivary proteins that bound to grass phytoliths, bovine dental enamel and dentine

Protein name	Matching species	Protein accession no. (NCBI)	Total protein score	Peptides matched in MS/MS	Molecular weight ($\times 10^3$)	Sequence coverage (%)
Lactoperoxidase	*Bos taurus*	P80025	171	DSLQKVSFSR EQINAVTSFLDASLVYGSEPSLASR FGHMEVPSTVSR IIKDGGIDPLVR IVGYLDEEGVLDQNR TPDNIDIWIGGNAEPMVER	80.59	13
Carbonic anhydrase VI (CA-VI)	*Bos taurus*	P18915	175	DLDIQDMLPGDLR DYAENTYYSNFISHLEDIR QGEFPMTNNGHTVQISLPSSMR VVEANFVSHPHQEYTLGSK YGSYEEAQNEPDGLAVLAALVEVK	36.98	30
BSP30	*Bos taurus*	P79124	260	GLGTFDSTIEIIQNLK KLIGEPQVTTQQEI LDLNVDLQTSVSIETDAETGDSR LIGEPQVTTQQEI RLISGLER	26.37	33
Odorant-binding protein (OBP)	*Bos taurus*	P07435	555	RPGLLNDVVDFGVNLVR AQEEEAEQNLSELSGPWR ATKQDDTYVADYEGQNVFK ELVFDDEKGTVDFYFSVK LNVEDEDLEK LNVEDEDLEKFNK NVVNFLENEDHPHPE QDDGTYVADYEGQNVFK THLVAHNINVDK TVYIGSTNPEK	18.49	67
Haemoglobin β	*Bos taurus*	P02070	354	AAVTAFWGK EFTPVLQADFQK FFESFGDLSTADAVMNNPK LLVVYPWTQR NFGKEFTPVLQADFQK VKVDEVGGEALGR VLDSFSNGMK VVAGVANALAHR	15.94	61

also with environmentally derived silicates (phytoliths, grit). Especially the interaction of carbonic anhydrases with those silicates could have a major impact on oral pH homeostasis, reducing the enzymatic activity and thereby increasing the chance of tooth damage due to acids originating from herbage and soil, as it has been stated and observed earlier in sheep throughout New Zealand (Michum & Bruere, 1984; Bloxham & Purton, 1991). Based on that, we wish to hypothesize that if the teeth were softened by dietary acids, dental wear caused by phytoliths and grit might be increased.

Nevertheless, future investigations are needed concerning the role of silicates and dietary acids in causing tooth damage in grazing farm animals. More emphasis should be put on the interaction of salivary proteins with environmental silicates as reactive or inhibiting surfaces in regard to salivary enzyme functions. Furthermore, it will be very interesting to know, if similar decay processes occur in wild-ranging grazers or if they have salivary countermeasures to prevent excessive tooth damage.

Acknowledgment: This work represents publication no. 52 of the DFG Research Unit 771 “Function and enhanced efficiency in the mammalian dentition - phylogenetic and ontogenetic impact on the masticatory apparatus”. We thank R. Pfuhl and G. Klautschek of FBN Dummerstorf, Germany for providing bovine saliva. Special thanks also to K. Weidemann, Zoological Institute of University Greifswald, Germany, for his help with the diamond saw to cut the bovine jaws and teeth. Furthermore, we acknowledge B. Heitkönig, B. Gehrig and B. Mielenz, Institute of Animal Science (University of Bonn), for their technical assistance. Many thanks also go to T.T. Wheeler (AgResearch New Zealand) for his help and suggestions during the preparation of the manuscript.

References

Ang CS, Binos S, Knight MI, Moate PJ, Cocks BG, McDonagh MB. 2011. Global survey of the bovine salivary proteome: integrating multidimensional prefractionation, targeted, and glycocapture strategies. *Journal of Proteome Research,* **10**(11): 5059-5069.

Asari M, Sasaki K, Kano Y, Nishita T. 1989. Immunohistochemical localization of carbonic anhydrase isozymes I, II and III in the bovine salivary glands and stomach. *Archives of Histology and Cytology,* **52**(4): 337-344.

Asari M, Miura K, Ichihara N, Nishita T, Amasaki H. 2000. Distribution of carbonic anhydrase isozyme VI in the developing bovine parotid gland. *Cells Tissues Organs,* **167**(1): 18-24.

Baker G, Jones LHP, Wardrop ID. 1959. Cause of wear in sheep's teeth. *Nature,* **184**(4698): 1583-1584.

Bloxham GP, Purton DG. 1991. Demineralisation and incisor wear: An *in vitro* study. *New Zealand Journal of Agricultural Research,* **34**(3): 277-279.

Dowd FJ. 1999. Saliva and dental caries. *Dental Clinics of North America,* **43**(4): 579-597.

Everest MA, Black VM, Haehlen AS, Haveman GA, Kliewer CJ, Neill HA. 2006. Hemoglobin adsorption to silica monitored with polarization-dependent evanescent-wave cavity ring-down spectroscopy. *The Journal of Physical Chemistry B,* **110**(39): 19461-19468.

Grantham MC, Dove PM. 1996. Investigation of bacterial-mineral interactions using Fluid Tapping Mode™ Atomic Force Microscopy. *Geochimica et Cosmochimica Acta,* **60**(13): 2473-2480.

Guiraudie G, Pageat P, Cain AH, Madec I, Nagnan-Le MP. 2003. Functional characterization of olfactory binding proteins for appeasing compounds and molecular cloning in the vomeronasal organ of pre-pubertal pigs. *Chemical Senses,* **28**(7): 609-619.

Haigh B, Hood K, Broadhurst M, Medele S, Callaghan M, Smolenski G, Dines M, Wheeler T. 2008. The bovine salivary proteins BSP30a and BSP30b are independently expressed BPI-like proteins with anti-*Pseudomonas* activity. *Molecular Immunology,* **45**(7): 1944-1951.

Healy WB, Ludwig TG. 1965. Wear of sheep's teeth. 1. The role of ingested soil. *New Zealand Journal of Agricultural Research,* **8**(4): 737-752.

Healy WB, Cutress TW, Michie C. 1967. Wear of sheep's teeth. IV. Reduction of soil ingestion and tooth wear by supplementary feeding. *New Zealand Journal of Agricultural Research,* **10**(2): 201-209.

Hummel J, Findeisen E, Südekum K-H, Ruf I, Kaiser TM, Bucher M, Clauss M, Codron D. 2011. Another one bites the dust: faecal silica levels in large herbivores correlate with high-crowned teeth. *Proceedings of the Royal Society B: Biological Sciences,* **278**(1712): 1742-1747.

Kaplan MD, Baum BJ. 1993. The functions of saliva. *Dysphagia,* **8**(3): 225-229.

Karlsson M, Mårtensson LG, Jonsson BH, Carlsson U. 2000. Adsorption of human carbonic anhydrase II variants to silica nanoparticles occur stepwise: Binding is followed by successive conformational changes to a molten-globule-like state. *Langmuir,* **16**(22): 8470-8479.

Ludwig TG, Healy WB, Cutress TW. 1966. Wear of sheep's teeth. III. Seasonal variation in wear and ingested soil. *New Zealand Journal of Agricultural Research,* **9**(2): 157-164.

Lundqvist M, Sethson I, Jonsson BH. 2004. Protein adsorption onto silica nanoparticles: Conformational changes depend on the particles' curvature and the protein stability. *Langmuir,* **20**(24): 10639-10647.

Madella M, Alexandre A, Ball T. 2005. International code for phytolith nomenclature 1. 0. *Annals of Botany,* **96**(2): 253-260.

Mau M, Kaiser TM, Südekum K-H. 2010. Carbonic anhydrase II is secreted from bovine parotid glands. *Histology and Histopathology,* **25**(3): 321-329.

Mau M, Müller C, Langbein J, Rehfeldt C, Hildebrandt JP, Kaiser TM. 2006. Adhesion of bovine and goat salivary proteins to dental enamel and silicate. *Archiv Tierzucht/Archives Animal Breeding,* **49**(5): 439-446.

McNaughton SJ, Tarrants JL. 1983. Grass leaf silicification: Natural selection for an inducible defense against herbivores. *Proceedings of the National Academy of Sciences United States of America,* **80**(3): 790-791.

Mera MU, Beveridge TJ. 1993. Mechanism of silicate binding to the bacterial cell wall in *Bacillus subtilis*. *Journal of Bacteriology,* **175**(7): 1936-1945.

Michum GD, Bruere AN. 1984. Solubilisation of sheep's teeth: A new look at a widespread New Zealand problem. In: Proceedings of the 14th Seminar of the Society of Sheep and Beef Cattle Veterinarians of the New Zealand Veterinary Association, 44-56.

Parr JF, Dolic V, Lancaster G, Boyd WE. 2001. A microwave digestion method for the extraction of phytoliths from herbarium specimens. *Review of Palaeobotany and Palynology,* **116**(3-4): 203-212.

Sanson GD, Kerr SA, Gross KA. 2007. Do silica phytoliths really wear mammalian teeth? *Journal of Archaeological Science,* **34**(4): 526-531.

Svendsen IE, Lindh L, Arnebrandt T. 2006. Adsorption behaviour and surfactant elution of cationic salivary proteins at solid/liquid interfaces, studied by *in situ* ellipsometry. *Colloids & Surfaces B: Biointerfaces,* **53**(2): 157-166.

Tabak LA. 1995. In defense of the oral cavity: structure, biosynthesis, and function of salivary mucins. *Annual Review of Physiology,* **57**(1): 547-564.

Takami S. 2002. Recent progress in the neurobiology of the vomeronasal organ. *Microscopy Research and Technique,* **58**(3): 228-250.

Tegoni M, Ramoni R, Bignetti E, Spinelli S, Cambillau C. 1996. Domain swapping creates a third putative combining site in bovine odorant binding protein dimer. *Nature Structural Biology,* **3**(10): 863-867.

Urabe Y, Shiomi T, Itoh T, Kawai A, Tsunoda T, Mizukami F, Sakaguchi K. 2007. Encapsulation of hemoglobin in mesoporous silica (FSM)-enhanced thermal stability and resistance to denaturants. *ChemBioChem,* **8**(6): 668-674.

Wheeler TT, Haigh BJ, Broadhurst MK, Hood KA, Maqbool NJ. 2011. The BPI-like/PLUNC family proteins in cattle. *Biochemical Society Transactions,* **39**(4): 1006-1011.

Cytotoxicity and genome-wide microarray analysis of intestinal smooth muscle cells in response to hexavalent chromium induction

Li-Fang JIN, Yuan-Yuan WANG, Zi-Dong ZHANG, Yi-Meng YUAN, Yi-Rui HU, Yang-Feng WEI, Jian NI*

College of Life Science of Shaoxing University, Shaoxing Zhejiang 312000, *China*

Abstract: Chronic ingestion of high concentrations of hexavalent chromium [Cr(VI)] in drinking water induces intestinal tumors in mice; however, information on its toxicity on intestinal smooth muscle cells is limited. The present study aimed to assess the *in vitro* and *in vivo* toxicological effects of Cr(VI) on intestinal smooth muscle cells. Human intestinal smooth muscle cells (HISM cells) were cultured with different concentrations of Cr(VI) to evaluate effects on cell proliferation ability, oxidative stress levels, and antioxidant system. Furthermore, tissue sections in Cr(VI) exposed rabbits were analyzed to evaluate toxicity on intestinal muscle cells *in vivo*. Gene chips were utilized to assess differential gene expression profiles at the genome-wide level in 1 μmol/L Cr(VI) treated cells. Intestinal tissue biopsy results showed that Cr(VI) increased the incidences of diffuse epithelial hyperplasia in intestinal jejunum but caused no obvious damage to the structure of the muscularis. Cell proliferation analysis revealed that high concentrations (≥64 μmol/L) but not low concentrations of Cr(VI) (≤16 μmol/L) significantly inhibited the growth of HISM cells. For oxidative stress levels, the expression of reactive oxygen species (ROS) and nitric oxide (NO) was elevated at high concentrations (≥64 μmol/L) but not at low concentrations of Cr(VI) (≤16 μmol/L). In addition, dose-dependent increases in the activity of oxidized glutathione (GSSH)/total-glutathione (T-GSH) were also observed. Gene chip screened 491 differentially expressed genes including genes associated with cell apoptosis, oxidations, and cytoskeletons. Some of these differentially expressed genes may be unique to smooth muscle cells in response to Cr(VI) induction.

Keywords: Intestinal smooth muscle cells; Hexavalent chromium; Cytotoxicity; Gene chip

Heavy metals toxin exposure can impact human and animal health (Liu et al, 1991; Smith, 2008). Hexavalent chromium [Cr(VI)] is considered carcinogenic to humans (Group 1) by the International Agency for Research on Cancer (IARC) and evidence on lung carcinogenic effects of Cr(VI) has been fully described in previous reports (Park & Stayner, 2006; Smith, 2008). In addition, epidemiologic studies have indicated that exposure to Cr(VI) may damage the liver (Rafael et al, 2007; Yuan et al, 2012), kidneys (Velma & Tchounwou, 2011), reproductive system (Subramanian et al, 2006), and immune system (Raghunathan et al, 2009). Hexavalent chromium can be inhaled or administered intratracheally, intraperitoneally, intravenously, or orally. Oral ingestion of contaminated foods and drinking well-water is the main source of non-occupational exposure to Cr(VI). Previous research has shown that human population exposure to Cr(VI) in drinking water resulted in a statistically significant increase in stomach tumors (Zhang & Li, 1997). More recently, administration to rodents of Cr(VI) in drinking water resulted in statistically significant increases in papillomas and carcinomas (combined) of the oral cavity and small intestine in high dose groups (Stout et al, 2009). To further elucidate key events underlying toxicity of Cr(VI) on the intestine, Kopec et al (2012) analyzed differential gene expression patterns in intestinal samples following 7 or 90 days exposure to different concentrations of Cr(VI) in drinking water, and showed expression levels of genes related to oxidative stress, cell cycle, lipid metabolism, and immune response changed in a dose-dependent way with Cr(VI) exposure. These results strongly suggest that Cr(VI) escaping from stomach reduction could be toxic to the gastrointestinal tract by

Received: 26 November 2012; Accepted: 10 January 2013
Foundation items: Zhejiang Natural Sciences Foundation Y2110911
* Corresponding author, E-mail: nijian@usx.edu.cn

changing the expression level of genes.

Intestinal smooth muscle cells provide structural support for many tissues and control essential physiological processes such as gastrointestinal motility and blood pressure. In digestive systems, rings of smooth muscle, called sphincters, regulate movement of materials along internal passageways and push contents through the central lumen. Studies have suggested that Cr(VI) has an adverse effect on intestinal epithelial tissue/cells; so far, however, available information on toxicity effects of Cr(VI) on intestinal smooth muscle cell is limited. Because Cr(VI) as chromate structurally resembles sulfate and phosphate, it can be taken up by all cells and organs throughout the body through nonspecific anion transporters. In addition, the expression of genes in a given cell is very different compared to those expressed in the other cells. Therefore, Cr(VI) may induce unique gene expression patterns for a given cell. Microarray analysis can provide quantitative gene expression information at the genome-wide level and help discover novel changes in genes expression, which may be unique to given cells. Therefore, the purpose of our study was to evaluate the effect of Cr(VI) on the cytotoxicity of intestine smooth muscle cells, and screen differentially expressed genes to identify novel changes in gene expression profiles by gene chip in intestinal smooth muscle cells in response to Cr(VI) induction.

MATERIALS AND METHODS

Animal model design

Groups of 12 male and 12 female New Zealand white rabbits were exposed to potassium dichromate ($K_2Cr_2O_7$) in drinking water at concentrations of 0, 7, or 41.8 mg/L Cr(VI) for 3 months (equivalent to average daily doses of approximately 0, 0.35, and 2.09 mg Cr(VI)/kg body weight per day per rabbit). Animals were observed twice daily and clinical findings were recorded. After exposure to Cr(VI) for 3 months, jejuna of the intestines were fixed and preserved in 10% neutral buffered formalin, trimmed and processed, embedded in paraffin, sectioned to a thickness of 4–6 μm, and stained with hematoxylin and eosin (H&E) for microscopic examination (Nikon, Japan). The Institutional Animal Care and Use Committee(s) (IACUC) at the College of Life Science of Shaoxing University approved all procedures performed on the animals (approval number: S20110018).

Cell Culture

Human intestinal small muscle cells (HISM cells) from the American Type Culture Collection (ATCC) were cultured in DMEM (Invitrogen, CA) supplemented with 10% FBS (Hyclone, UT), 100 U/mL penicillin (Invitrogen, CA), and 100 mg/ml streptomycin (Invitrogen, CA). Cells were cultured at 37 °C in an incubator with a humidified atmosphere containing 5% CO_2. Media were changed every other day, and cells were split every 4 days. For Cr (VI) exposure, cells were exposed to 0, 0.25, 1, 4, 16, 64, and 128 μmol/L Cr(VI).

3-(4,5-cimethylthiazol-2yl)-2,5-diphenyl tetrazolium bromide (MTT) assay

Cells at the growth log phase for each group were inoculated into 96-well plates at 100 μL/well. Ten microliters of MTT (5 mg/mL) was added to each well before termination. Plates were incubated at 37 °C in 5% CO_2 for 4 h. The supernatant was discarded and DMSO (100 μL/well) was added. The mixtures were shaken gently to dissolve the hyacinth in sediment. Absorbance (A) values at a wavelength of 492 nm were detected by a microplate reader (Authos, Austria), and the cell proliferation rate was then calculated.

Cell growth curve assay

Briefly, 1×10^4/L cells in the logarithmic growth phase were harvested and seeded on 12-well plates overnight. Different concentration (0, 0.25, 1, 4, 16, 64, and 128 μmol/L) of Cr(VI) was administrated into the culture medium, and the cells were further incubated for 4 days. After incubation, cell viability was determined by trypan blue dye exclusion. A growth curve was drawn according to the logarithmic number of cells/L with incubation time. Multiplication time and growth saturation density were calculated based on the curve.

Measurement of nitric oxide (NO) production

After culturing with different concentrations (0, 0.25, 1, 4, 16, 64, and 128 μmol/L) of Cr(VI) for 30 min, total NO production was estimated by spectrophotometric measurement of nitrite and nitrate concentrations in the cell culture supernatant fluid using Griess reagent with the Total Nitric Oxide Assay Kit (Beyotime Ins. Bio, China) according to manufacturer's instructions. Optical density at 540 nm was measured by a microplate reader (Authos, Austria). Concentrations were calculated by comparing absorptions with those of the standard curve.

Determination of cellular reactive oxygen species (ROS)

To determine intracellular accumulation of ROS in HISM cells, the membrane permeable indicator dihydrodichlorofluorescein diacetate (H2DCF-DA) (Nanjing Jiancheng Corp, China) was employed. The HISM cells treated with Cr(VI) for 24 h were loaded with 10 μmol/L H2DCF-DA in serum-free medium at 37 °C for 90 min, and then washed twice with PBS and digested by trypsin. Cells were monitored with an inverted fluorescence microscope (Nikon, Japan) at an

excitation wavelength of 488 nm and an emission wavelength of 525 nm. Reactive oxygen species were determined by comparing changes in fluorescence intensity with those of the standard curve.

Oxidized glutathione (GSSH)/total-glutathione (T-GSH) assay

The HISM cells treated with Cr(VI) for 24 h were lysed using liquid nitrogen and GSSH/T-GSH activity was evaluated in cells using the glutathione peroxidase assay kit (Nanjing Jiancheng Corp, China), according to manufacturer's instructions. This assay is based on the oxidation of NADPH to NAD+, catalyzed by a limiting concentration of glutathione reductase, with maximum absorbance at 340 nm by the microplate reader (Authos, Austria).

Microarray hybridization and data analysis

Microarray analysis was conducted using Agilent Human Whole Genome 8×60 k Arrays to analyze ~40 000 transcripts. Total RNA from 1 μmol/L Cr(VI) treated or untreated samples was isolated with Trizol reagent (Invitrogen) and then stored at −80 °C. Fifty nanograms of total RNA was converted into labeled cRNA with nucleotides coupled to fluorescent (Cy3) dye using the Quick Amp Kit (Agilent Technologies, Palo Alto, CA) following the manufacturer's protocols. The A260/280 nm ratio and yield of each of the cRNAs were determined and quality assessment was done using an Agilent Bioanalyzer. Equal amounts of Cy3-labeled cRNA from two different samples were hybridized to Agilent Human Whole Genome 8×60 k Microarrays. The hybridized array was washed and scanned and data were extracted from the scanned image using Feature Extraction version 10.2 (Agilent Technologies). Microarray data were normalized using a semi-parametric approach. Unless stated otherwise, gene expression data were ranked and prioritized using fold change>2 criteria to identify differentially expressed genes. Annotation and functional categorization of differentially regulated genes were performed using the Database for Annotation, Visualization and Integrated Discovery (DAVID) and Ingenuity Pathway Analysis (IPA, Ingenuity Systems, Red wood City, CA).

Quantitative reverse transcription polymerase chain reaction (qRT-PCR)

Samples of total RNA were isolated from cells used in microarray hybridization using SYBR Green-based qRT-PCR. Briefly, 0.5 μg of RNA was primed by Oligo$(dT)_{16}$ (Promega, USA) and reverse transcribed using AMV reverse transcriptase in a 20 μL reaction system. From a 2-fold dilution of this cDNA solution, 0.5 μL was used in a 20 μL PCR reaction containing 10 μL SYBR premix Ex Taq, 0.4 μL Rox (TaKaRa, Japan), and 10 μmol/L forward and reverse primers. All primers were designed by submitting RefSeq sequences to Primer Premier 5.0 software; amplicons were approximately 100–200 bp. Primer sequence for MPRIP is 5′-GCTTGGAGGTGCCATATAC-3′/5′-GACCGTTCACTG GATGAAA-3′; for ACTR3B is 5′-CCGCTGTATAA GCCCGAGTT-3′/5′-CAACGTGACACCATCGAACG-3′; for ACTIN is 5′-AGCCTCGCCTTTGCCGATCC-3′/5′-ACATGCCGGAGCCGTTGTCG-3′. The PCR amplifications were conducted in 96-well BIOplastics (Axygen, USA) on an Applied Biosystems PRISM 7300 Sequence Detection System under the following conditions: 10 seconds denaturation and enzyme activation at 95 °C, followed by 40 cycles of denaturation (95 °C, 10 seconds), and annealing (60 °C, 30 seconds). Results were normalized to beta-actin to control for differences in RNA loading, quality, and cDNA synthesis. Amplicon size and reaction specificity were confirmed by agarose gel electrophoresis. Each sample was assayed in triplicate and median threshold cycle values were used to calculate the fold change between treated and control samples.

Statistical Analysis

All data were expressed as means±*SEM*. Statistical comparisons were performed using Student's *t*-test, $P<0.05$ was considered statistically significant.

RESULTS AND DISCUSSION

Intestinal tissue biopsy

The aim of this study was to assess the toxicity of Cr(VI) on intestinal tissue. Intestine sections from rabbits, which ingested Cr(VI)-containing water for 3 months, were proceeded and observed. Consistent with previous studies (Bucher, 2007; Thompson et al, 2011), our results showed a clear exposure concentration response for increased incidences of diffuse epithelial hyperplasia in intestinal jejuna (Figure 1A, 1B, 1C). In the control group, intestinal mucosa was lined with a continuous layer of polarized epithelial cells (Figure 1A1). In contrast, exposure to Cr(VI) resulted in disruption of intestinal epithelial tissue integrity and disorder of the linear arrangement of epithelial cells (Figure 1B1, C1). In contrast to the controls (Figure 3A), the jejuna of the Cr(VI) exposed rabbits had short, broad, blunt epithelial cell layers and generalized mucosal hypercellularity that was particularly prominent in the mucosa crypt (Figure 1A2, B2, C3). Muscularis of the small intestine consists of smooth muscle fibers, and we did not find obvious changes in morphology, muscle fibers and cell nuclei in Cr(VI) induced muscularis tissue compared with those in the untreated group (Figure 1A3, B3, C3).

For the first time, this study provided additional evidence that Cr(VI) was responsible for intestinal

hyperplasia in the rabbit model. However, obvious changes were not found in the morphology, muscle fibers, and cell nuclei of the muscularis in response to Cr(VI) induction, which may be partially explained as: (1) most Cr(VI) escaping from stomach reduction were absorbed by intestinal epithelial cells before penetrating into the muscularis, which resulted in low concentration of Cr(VI) in smooth muscle cells; (2) compared to intestine epithelial cells, smooth muscle cells were not sensitive to toxicity or carcinogenicity of Cr(VI); and or (3) toxicity of Cr(VI) on intestine muscularis was not well reflected at the tissue level.

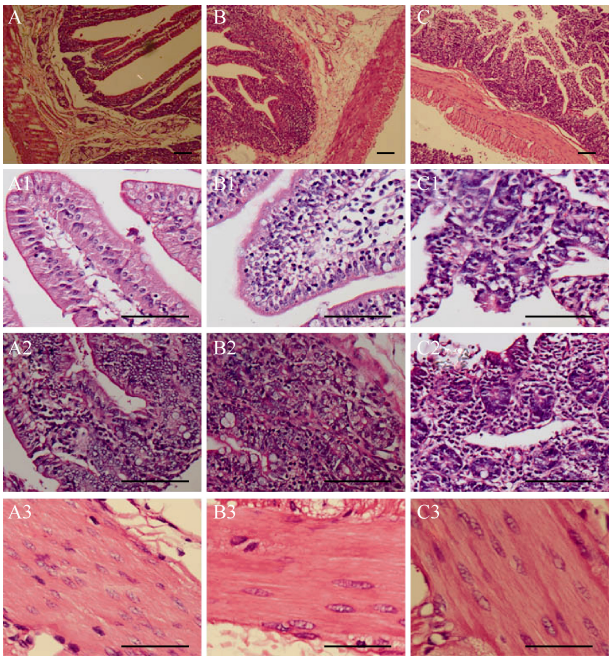

Figure 1 *in vivo* analysis on toxicity of Cr(VI) (0 mg/L (A, A1, A2, A3), 7 mg/L (B, B1, B2, B3) and 41.8 mg/L (C, C1, C2, C3)) on adult rabbit intestines

Low magnification micrograph of small intestine showed diffuse epithelial hyperplasia in jejunum of the 7 mg/L (B) and 41.8 mg/L (C) Cr(VI) treated groups compared to untreated group (A). In contrast to the controls (A1), exposure to Cr(VI) (B1, and C1) resulted in disruption of epithelial arrangement of mucosa. High magnification micrograph of small intestine mucosa showed a short, broad, blunt epithelial cell layer and generalized mucosal hypercellularity in the mucosa crypt in the 7 mg/L (B2) and 41.8 mg/L (C2) Cr(VI) treated groups compared to untreated group (A2). No changes were observed in morphology, muscle fibers and cell nuclei of smooth muscle cells, and thickness of muscularis in Cr(VI) treated or untreated groups (A3, B3 and C3). All sections were stained with hematoxylin and eosin. Bar=200 μm.

Effect of Cr(VI) on cell viability and proliferation

To further study the potential toxic effect of Cr(VI) on smooth muscle cells, we tested the effect of Cr(VI) on the morphology and proliferation of human intestinal small muscle cells (HISM cells) at the cellular level. After treatment with different concentrations (0, 0.25, 1, 4, 16, 64, and 128 μmol/L) of Cr(VI) for 24 hours, the morphology of HISM cells was observed under an inverted phase contrast microscope. At low concentrations of Cr(VI) (≤16 μmol/L), cells maintained a long spindle-shaped fibrocyte-like morphology. However, cells shrunk and became round at high concentrations of Cr(VI) (≥64 μmol/L) (Figure 2A). The MTT assay further revealed that low concentrations of Cr(VI) (≤16 μmol/L) had no effect on cell proliferation, but high concentrations of Cr(VI) (≥64 μmol/L) significantly weakened cell proliferation ability (Figure 2B). Consistent with the MTT assay results, the cell growth curve also showed that high concentrations of Cr(VI) (≥16 μmol/L) decreased the number of HISM cells in a time-dependent manner (Figure 2C). Taken together, consistent with previous studies (Ye & Shi, 2001; Kimura et al, 2011), our results suggest that moderate to high concentrations of Cr(VI) were toxic to HISM cell proliferation.

Detection of ROS and NO

Both ROS and NO play important roles in many cellular signaling pathways, such as proliferation, cell activation, and migration. They can be detrimental when produced in high amounts in intracellular compartments, which is also referred to as “oxidative and nitrosative stress” (Myers et al, 2011). Therefore, experiments were designed to detect the expression levels of ROS and NO in cells with short-term Cr(VI) induction. We found that high concentrations of Cr(VI) (≥64 μmol/L) significantly increased the production of ROS and NO (Figure 3A). In contrast, low concentrations of Cr(VI) (≤16 μmol/L) failed to increase ROS and NO production in HISM cells (Figure 3B). Thus, these results revealed that exposure to high concentrations of Cr(VI) (≥64 μmol/L) resulted in an excessive increase in ROS and NO generation in HISM cells, which could induce cell death as confirmed by cell proliferation analysis.

Assay of GSSH/T-GSH

Cells have an elaborate defense system, such as GSSH/T-GSH, against injurious oxidizing agents. This system helps to maintain steady state concentrations of active oxygen at acceptable levels under physiological conditions. In contrast, inhibition of this defense system can induce a prooxidant state (Myers et al, 2011; Shi & Jiang, 2002). In the present study, the expression levels of GSSH/T-GSH were detected to evaluate the activity of antioxidant systems in Cr(VI) induced cells. After treatment with different concentrations of Cr(VI) for 24 h, activity of GSSH/T-GSH (Figure 3C) increased in a dosage-dependent manner. Increased expression of GSSH/T-GSH indicated that cellular antioxidant systems were activated in response to Cr(VI) to remove extra O^-_2 and H_2O_2.

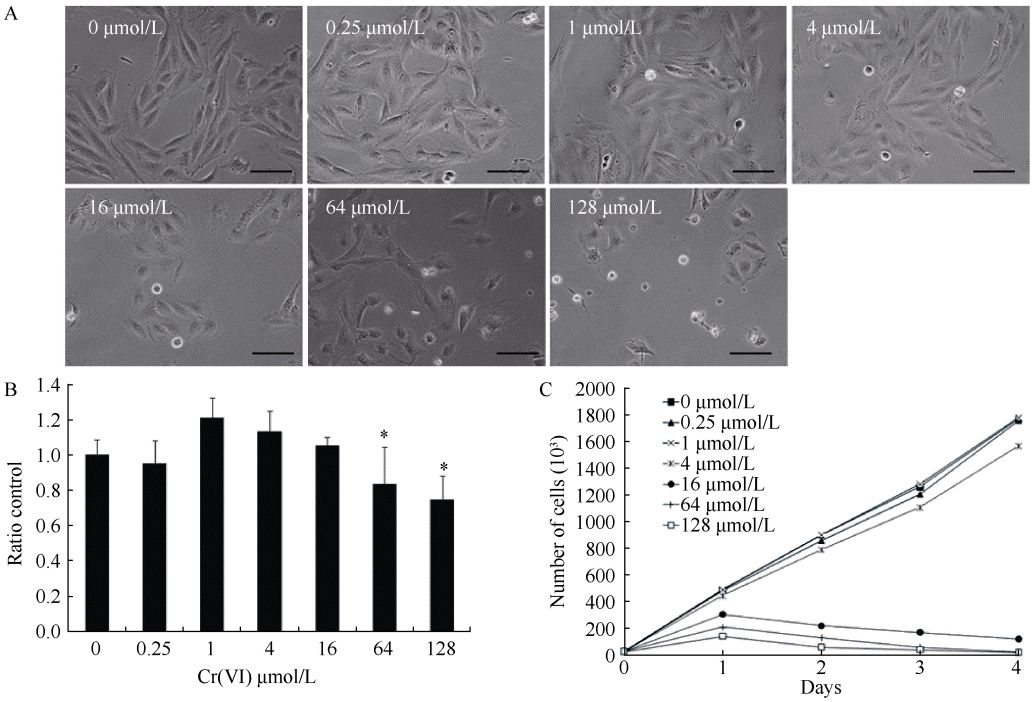

Figure 2 Effect of Cr(VI) on cell morphology and cell number

A: Phase contrast images of HISM cells treated with or without different concentration of Cr(VI); MTT (B) and growth curves (C) assay revealed that high concentration of Cr(VI), but not low concentration of Cr(VI), inhibited growth rate of HISM cells. Data are expressed as means±*SEM* of three independent experiments, *:P<0.05, compare to control group. Bar=100 μm.

Functional annotation and pathway analysis of differentially expressed genes

To investigate gene expression information at the genome-wide level, we analyzed gene expression profiles in HISM cells after exposure to 1 μmol/L Cr(VI) using Agilent human whole genome Microarray Kit. In comparison to control cells, 196 genes were significantly upregulated and 295 genes were significantly downregulated (fold >2). To assess the biological relevance of the differentially expressed genes, we loaded the gene expression data into GeneSpring to sort differentially expressed genes into determined gene ontology groups. Gene ontology (GO) terms and Kyoto Encyclopedia of Genes and Genomes (KEGG) pathways with significant over-representation are listed in Table 1.

The 491 differentially expressed genes were then classified into different functional categories according to the GO project for biological process. The main GO categories for differentially expressed genes were related to cell differentiation, protein homoligomerization, positive regulation of protein phosphorylation, mitochondrion organization, sensory perception of taste, endoplasmic reticulum to Golgi vesicle-mediated transport, smooth muscle contraction, and carbohydrate transport. The KEGG pathway analysis component was used to find co-expressed clusters sharing the same pathway. Six signaling pathways were found to be involved in protein processing in endoplasmic reticulum and leukocyte transendothelial migration (Table 1). Therefore, we provided a global view of differential gene expression in HISM cells in response to Cr(VI) induction.

Changes in genes associated with cell apoptosis, actin cytoskeleton, and oxidation

We identified specific genes of interest within the cluster groups. Genes associated with apoptosis, oxidations, and cytoskeletons, and their differential expression patterns are shown in Table 2. Most proapoptosis related genes were downregulated; for example, KLF6 was downregulated 5.66 times, CASP10 was downregulated 4.41 times, and NLRP1 was downregulated 4.25 times. Decreased expression level of apoptosis related genes partially explained the survival and proliferation of HISM cells after exposure to low concentrations of Cr(VI). As previously described (Ye & Shi, 2001, Sun et al, 2011), changes in genes related to oxidative stress in our Cr(VI) exposed cells were also observed, such as NOX4 and MSRB2. Induction of genes associated with oxidative stress explains why there were changes in oxidation and antioxidant systems in HISM cells in response to Cr(VI).

It is worth noting that genes related to smooth muscle contraction changed, including the downregulation of MPRIP (5.20 times) and the upregulation of TTN and

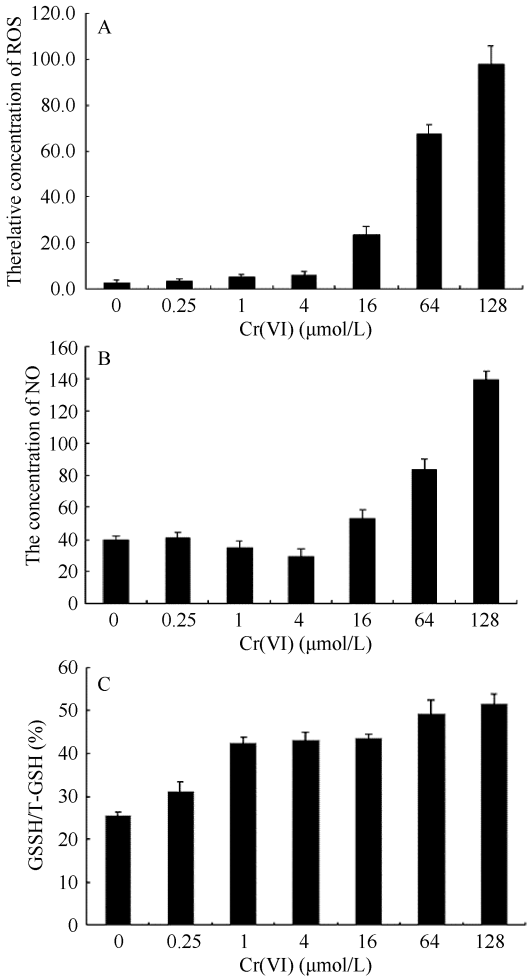

Figure 3 Detection expression level of ROS, NO and GSSH/T-GSH with different concentrations of Cr(VI).

Detection expression levels of ROS, NO and GSSH/T-GSH with different concentrations of Cr(VI). Cr(VI) treatment, especially high dose of Cr(VI) (≥64 μmol/L), increased ROS (A) and NO (B) expression level in HISM cells. Activity of GSSH/T-GSH (C) was unregulated in a dosage-dependent manner. Data were expressed as means±*SEM* of three independent experiments.

MYL7 (2.97 and 2.89 times, respectively). The MPRIP gene targets myosin phosphatase to the actin cytoskeleton through the regulation of actin cytoskeleton by RhoA and ROCK 1. Depletion of MPRIP leads to an increased number of stress fibers in smooth muscle cells through stabilization of actin fibers by phosphorylated myosin. In addition, overexpression of MPRIP as well as its F-actin-binding region leads to disassembly of stress fibbers in neuronal cells (Koga & Ikebe, 2005; Surks et al, 2005). Our data suggested that Cr(VI) may have a potential role in the contraction of smooth muscle cells.

Real time PCR validation of gene expression

To validate our microarray study results, qRT-PCR was performed on a subset of two genes exhibiting a

Table 1 Functional annotation and pathway analysis of genes more than 2-fold in 1 μmol/L Cr(VI) treated cells

Category	GO Term	List hits	*P*-value
GO Biological Process	Cell differentiation	14	0.0438
	Protein homooligomerization	4	0.0402
	Positive regulation of protein phosphorylation	4	0.0199
	Mitochondrion organization	4	0.0012
	Sensory perception of taste	4	0.00311
	ER to Golgi vesicle-mediated transport	3	0.0384
	Smooth muscle contraction	3	0.000948
	Carbohydrate transport	3	0.0167
	COPII vesicle coating	2	0.00955
	Calcium-independent cell-cell adhesion	2	0.0487
	Cardiac muscle fiber development	2	0.00411
	Chondroitin sulfate biosynthetic process	2	0.00751
GO Cellular Component	Integral to membrane	88	0.0167
	Intracellular	44	0.0281
	Membrane fraction	14	0.0373
	Ribosome	9	0.0013
	Transport vesicle	3	0.0284
	Nicotinic acetylcholine-gated receptor-channel complex	2	0.0332
	ER to Golgi transport vesicle membrane	2	0.0262
	COPI coated vesicle membrane	1	0.0337
	SSL2-core TFIIH complex	1	0.017
	Telomeric heterochromatin	1	0.017
	NALP1 inflammasome complex	1	0.017
	Nuclear telomeric heterochromatin	1	0.0337
GO Molecular Function	Ion channel activity	7	0.0121
	Endonuclease activity	4	0.0216
	Extracellular ligand-gated ion channel activity	3	0.0405
	Folic acid binding	2	0.0249
	Nicotinic acetylcholine-activated cation-selective channel activity	2	0.0282
	Acetylcholine receptor activity	2	0.0189
	Acetylcholine binding	2	0.0136
	Carboxylic acid binding	2	0.00393
	Glycolipid binding	2	0.00544
	Taste receptor activity	2	0.0249
	Ribonuclease activity	2	0.0316
	Neuromedin U receptor activity	1	0.0329
KEGG Annotations	Protein processing in endoplasmic reticulum	6	0.0325
	Leukocyte transendothelial migration	5	0.0261
	Spliceosome	5	0.0365
	Taste transduction	5	0.000835
	alpha-Linolenic acid metabolism	2	0.0328
	Dorso-ventral axis formation	2	0.0495

Table 2 Genes related to cell proliferation, oxidation, and muscle contraction

Gene symbol	Gene name	Fold	Direction	Description
Genes related to cell proliferation				
KLF6	Kruppel-like factor 6	5.66	↓	Functions as a tumor suppressor
SIRT6	Sirtuin 6	5.13	↓	Modulates acetylation of histone H3 in telomeric chromatin during the S-phase of the cell cycle
CASP10	Caspase 10	4.41	↓	Involved in activation cascade of caspases responsible for apoptosis execution
NLRP1	Pyrin domain containing 1	4.25	↓	Enhances APAF1 and cytochrome c-dependent activation of pro-caspase-9 and consecutive apoptosis.
TNFAIP1	Tumor necrosis factor, alpha-induced protein 1	3.17	↓	Interaction with RHOB may regulate apoptosis, regulating actin cytoskeleton and cell migration
C1QTNF1	C1q and tumor necrosis factor related protein 1	3.26	↓	Function as a apoptosis factors
MAPK15	mitogen-activated protein kinase 15	2.04	↑	In vitro, phosphorylates MBP
RHOB	Rho-related GTP-binding protein	2.03	↓	Mediates apoptosis in neoplastically transformed cells after DNA damage.
Genes related to actin cytoskeleton				
ACTR3B	actin-related protein 3 homolog B	5.27	↑	Regulatory role in actin cytoskeleton and induces cell-shape change and motility.
MPRIP	myosin phosphatase Rho interacting protein	5.20	↓	Targets myosin phosphatase to actin cytoskeleton. Required for regulation of actin cytoskeleton by RhoA and ROCK1.
TTN	titin	2.97	↑	Key component in assembly and functioning of vertebrate striated muscles
MYL7	myosin, light chain 7	2.89	↑	Muscle contraction
NMUR1	neuromedin U receptor 1	2.14	↓	Receptor for neuromedin-U and neuromedin-S neuropeptides
EDNRA	endothelin receptor type A	2.14	↓	Receptor for endothelin-1.
Genes related to oxidation				
AIG1	androgen-induced 1	7.68	↑	Plays a role in androgen-regulated growth of hair follicles
NOX4	NADPH oxidase 4	2.70	↑	Constitutive NADPH oxidase which generates superoxide intracellularly upon formation of a complex with CYBA/p22phox
MSRB2	Methionine-R-sulfoxide reductase B2	2.28	↓	Plays a role in preservation of mitochondrial integrity by decreasing intracellular reactive oxygen species build-up through its scavenging role
FMO1	methylaniline monooxygenase	2.25	↓	Involved in oxidative metabolism of a variety of xenobiotics such as drugs and pesticides.
DHRS11	dehydrogenase/reductase	2.13	↓	Can utilize both NADH and NADPH

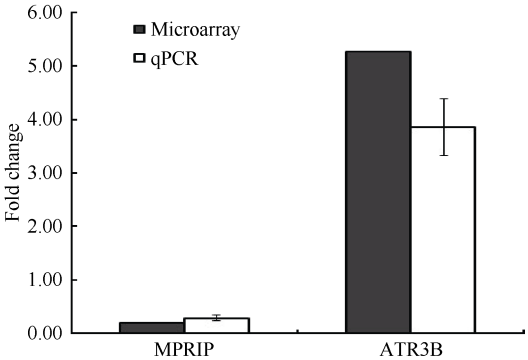

Figure 4 Comparisons between Q-polymerase chain reaction (qPCR) gene expression patter and microarray data between treated and control samples.

minimum 5-fold change in gene expression. Genes related to smooth muscle contraction such as ACTR3B and MPRIP were chosen based on their level of expression in the microarray study. As shown in Figure 4, the upregulated or downregulated patterns for ACTR3B and MPRIP obtained from qRT-PCR were similar to those in the microarray study.

CONCLUSION

The present work highlights the results of a series of in vitro studies, which demonstrated that oxidative stress and cytotoxicity were involved in the effect of Cr(VI) on HISM cells. In addition, here we provided a global view of differential gene expression in HISM cells in response to Cr(VI) induction and identified some novel changes in gene expression, such as MPRIP and TTN, that may be unique to smooth muscle cells in response to Cr(VI) induction. This study provides useful information not only for understanding molecular mechanisms in Cr(VI) toxicity, but also in advancing our knowledge in a number of fields.

References

Bucher J. 2007. NTP Toxicity Studies of Sodium Dichromate Dihydrate (CAS No. 7789-12-0) Administered in Drinking Water to Male and Female F344/N Rats and B6C3F1 Mice and Male BALB/c and am3-C57BL/6 Mice. *Toxicity Report Series,* (72): G1-G4.

Kimura T, Okumura F, Onodera A, Nakanishi T, Itoh N, Isobe M. 2011. Chromium (VI) inhibits mouse metallothionein-I gene transcription by modifying the transcription potential of the co-activator p300. *The Journal of Toxicological Sciences,* **36**(2): 173-180.

Koga Y, Ikebe M. 2005. p116Rip decreases myosin II phosphorylation by activating myosin light chain phosphatase and by inactivating RhoA. *The Journal of Biological Chemistry,* **280**(6): 4983-4991.

Kopec AK, Kim S, Forgacs AL, Zacharewski TR, Proctor DM, Harris MA, Haws LC, Thompson CM. 2012. Genome-wide gene expression effects in B6C3F1 mouse intestinal epithelia following 7 and 90days of exposure to hexavalent chromium in drinking water. *Toxicology and Applied Pharmacology,* **259**(1): 13-26.

Liu AH, He WS, Lin SY, Xiong XK, Zhao GF, Sun LH, Ji XM, Liu CL, Xuan XZ. 1991. Micronuclei of rat bone marrow cells and lung macrophages induced by five kinds of Yunnan Tin ore powder and four kinds of metallic compound. *Zoological Research,* **12**(3): 309-314. (in Chinese)

Myers JM, Antholine WE, Myers CR. 2011. The intracellular redox stress caused by hexavalent chromium is selective for proteins that have key roles in cell survival and thiol redox control. *Toxicology*, **281**(1-3): 37-47.

Park RM, Stayner LT. 2006. A search for thresholds and other nonlinearities in the relationship between hexavalent chromium and lung cancer. *Risk Analysis,* **26**(1): 79-88.

Rafael AI, Almeida A, Santos P, Parreira I, Madeira VM, Alves R, Cabrita AM, Alpoim MC. 2007. A role for transforming growth factor-beta apoptotic signaling pathway in liver injury induced by ingestion of water contaminated with high levels of Cr(VI). *Toxicology and Applied Pharmacology,* **224**(2): 163-173.

Raghunathan VK, Ellis EM, Grant MH. 2009. Response to chronic exposure to hexavalent chromium in human monocytes. *Toxicology in Vitro,* **23**(4): 647-652.

Shi D, Jiang BH. 2002. Antioxidant properties of apple juice and its protection against Cr(VI)-induced cellular injury. *Journal of Environmental Pathology Toxicology and Oncology,* **21**(3), 233-242.

Smith AH. 2008. Hexavalent chromium, yellow water, and cancer: a convoluted saga. *Epidemiology,* **19**(1): 24-26.

Stout MD, Herbert RA, Kissling GE, Collins BJ, Travlos GS, Witt KL, Melnick RL, Abdo KM, Malarkey DE, Hooth MJ. 2009. Hexavalent chromium is carcinogenic to F344/N rats and B6C3F1 mice after chronic oral exposure. *Environmental Health Perspectives,* **117**(5): 716-722.

Subramanian S, Rajendiran G, Sekhar P, Gowri C, Govindarajulu P, Aruldhas MM. 2006. Reproductive toxicity of chromium in adult bonnet monkeys (*Macaca radiata* Geoffrey). Reversible oxidative stress in the semen. *Toxicology and Applied Pharmacology,* **215**(3): 237-49.

Sun H, Clancy HA, Kluz T, Zavadil J, Costa M. 2011. Comparison of gene expression profiles in chromate transformed BEAS-2B cells. *PLoS One*, 6(3): e17982.

Surks HK, Riddick N, Ohtani K. 2005. M-RIP targets myosin phosphatase to stress fibers to regulate myosin light chain phosphorylation in vascular smooth muscle cells. *The Journal of Biological Chemistry,* **280**(52): 42543-4251.

Thompson CM, Proctor DM, Haws LC, Hebert CD, Grimes SD, Shertzer HG, Kopec AK, Hixon JG, Zacharewski TR, Harris MA. 2011. Investigation of the mode of action underlying the tumorigenic response induced in B6C3F1 mice exposed orally to hexavalent chromium. *Toxicological Sciences,* **123**(1): 58-70.

Velma V, Tchounwou PB. 2011. Hexavalent chromium-induced multiple biomarker responses in liver and kidney of goldfish, *Carassius auratus*. *Environmental Toxicology,* **26**(6): 649-656.

Ye J, Shi X. 2001. Gene expression profile in response to chromium-induced cell stress in A549 cells. *Molecular and Cellular Biochemistry,* **222**(1-2): 189-197.

Yuan Y, Ming Z, Gong HH, Lan G, Lu D, Peng L, Feng J, Zhong CG. 2012. Cr(VI) induces the decrease of ATP level and the increase of apoptosis rate mediated by ROS or VDAC1 in L-02 hepatocytes. *Environmental Toxicology and Pharmacology,* **34**(2): 579-587.

Zhang JD, Li SK. 1997. Cancer mortality in a Chinese population exposed to hexavalent chromium in water. *Journal of Occupational and Environmental Medicine,* **39**(4): 315-319.

Adaptation to visual stimulation modifies the burst firing property of V1 neurons

Rui-Long LIU[1], Ke WANG[1], Jian-Jun MENG[1], Tian-Miao HUA[1,*], Zhen LIANG[2,*], Min-Min XI[3]

1. *College of Life Sciences, Anhui Normal University, Wuhu* 241000*, China;*
2. *Department of Bio-Medical Engineering, Anhui Medical University, Hefei* 230032*, China;*
3. *Management School, Queen's University, UK*

Abstract: The mean firing rate of visual cortical neurons is reduced after prolonged visual stimulation, but the underlying process by which this occurs as well as the biological significance of this phenomenon remains unknown. Computational neuroscience studies indicate that high-frequency bursts in stimulus-driven responses can be transmitted across synapses more reliably than isolated spikes, and thus may carry accurate stimulus-related information. Our research examined whether or not adaptation affects the burst firing property of visual cortical neurons by examining changes in the burst firing changes of V1 neurons during adaptation to the preferred visual stimulus. The results show that adaptation to prolonged visual stimulation significantly decreased burst frequency (bursts/s) and burst length (spikes/burst), but increased burst duration and the interspike interval within bursts. These results suggest that the adaptation of V1 neurons to visual stimulation may result in a decrease of feedforward response gain but an increase of functional activities from lateral and/or feedback connections, which could lead to a reduction in the effectiveness of adapted neurons in transmitting information to its driven neurons.

Keywords: Visual adaptation; Burst firing; Neurons; Primary visual cortex; Cat

When exposed to prolonged stimulation, a neuron's response decreases gradually to a minimum firing level, a phenomenon called adaptation. Adaptation in the visual pathway is generally considered a property of visual cortical cells, though recent investigation showed that subcortical neurons also display a weaker adaptation to visual stimulation (Shou et al, 1996; Smirnakis et al, 1997; Baccus & Meister, 2002), and the primary visual cortex may undergo pattern-specific adaptation (Duong & Freeman, 2007). The mechanisms that underlie visual adaptation are still the subject of debate. Four possible hypotheses have been postulated, including contrast gain control (Carandini & Ferster, 1997; Sanchez-Vives et al, 2000), depression of excitatory synapses (Chung et al, 2002), strengthening of inhibitory synapses (Thomson & Deuchars, 1997) and neural network mechanism (Teich & Qian, 2003). However, these hypotheses do not provide sufficient evidence to explain adaptation properties reported by psychophysical experiments, likely because these proposals are based solely on analyses of mean firing rate, which cannot decode all the information (such as timing code) in the response of neurons to visual stimuli.

Additionally, the biological significance of visual adaptation is also unclear, though different views have been suggested (Kohn, 2007). A common concern within the proposed views is whether or not adaptation changes the efficiency of neuronal information encoding and perceptual discrimination. Several authors report that contrast adaptation may enhance contrast discrimination and information transmission (Greenlee & Heitger, 1988; Sharpee et al, 2006), while others found that the contrast

Received: 03 December 2012; Accepted: 20 February 2013
Foundation items: This work was supported by the National Natural Science Foundation of China (31171082), the Natural Science Foundation of Anhui Province (070413138), the Key Research Foundation of the Anhui Provincial Education Department (KJ2009A167), the Foundation of Key Laboratories of Anhui Province and the Anhui Provincial Education Department.
* Corresponding authors, E-mails: tmhua@mail.ahnu.edu.cn; liangzhen@foxmail.com

discrimination thresholds remained unchanged after adaptation (Maattanen & Koenderink, 1991). Still others argue that Greenlee and Heitger and Maattanen and Koenderink reach different conclusions because of respective differences in viewing conditions (Abbonizio et al, 2002). To resolve these disputes, we assessed the capacity changes of neurons in information encoding and transmitting during adaptation.

Recent studies in computational neuroscience indicate that a neuron's response is composed of two firing modes with different roles in information processing (Krahe & Gabbiani, 2004; Oswald et al, 2004). One is an isolated firing mode with a single action potential, or spike, separated by long interspike intervals (>20 ms). The other is called high-frequency burst firing (BF), which is a sequence of action potentials separated by short interspike intervals (<20 ms, mostly several ms). Because burst firing can induce two or more excitatory postsynaptic potentials (EPSPs) within a short time frame, and these EPSPs are more likely to excite the postsynaptic neuron, most of authors believe that burst firing can facilitate synaptic transmission more reliably than isolated firing, and thus carry faithful stimulus-specific information (Cattaneo et al, 1981; Eggermont & Smith, 1996; Lisman, 1997; Krahe & Gabbiani, 2004). In a certain sense, isolated firing could be considered as noise inherent in the neural circuits (Lisman, 1997).

An *in vivo* investigation has shown that burst firing has a significantly higher effectiveness than single isolated spike in eliciting a spike from a driven neuron, and that longer bursts are more effective than shorter ones (Snider et al, 1998). Furthermore, burst length (spikes/burst) and burst frequency (bursts/s) are modulated by changes of local intracortical inhibition. Iontophoretic application of GABA could significantly shorten burst length, whereas administration of bicuculline, an antagonist of $GABA_A$ receptor, increased burst length of the cell's response (DeBusk et al, 1997). In this research, we examined the changes of burst firing property of V1 neurons during adaptation to prolonged visual stimulation, attempting to find clues to the mechanisms that may mediate visual adaptation process as well as biological implications of adaptation.

MATERIALS AND METHODS

Subjects

Subjects for this study were four young adult cats (2−3 years old). Each subject was a healthy domestic cat with the history of age and healthcare properly documented by veterinarians. Subjects were examined ophthalmoscopically before experiment to confirm that no optical or retinal problems impaired their visual function. All experiment procedures were done strictly in accordance with the guidelines published in the NIH Guide for the care and use of Laboratory Animals.

Extracellular recording procedures

All subjects were prepared for extracellular single-unit recording using a procedure previously described (Hua et al, 2006; Hua et al, 2009; Hua et al, 2010). Briefly, anaesthesia was induced by injection (i.m) of ketamine HCl (40 mg/kg, im) and xylazine (2 mg/kg, im). After intubation of intravenous and tracheal cannulae, the cat was immobilized in a stereotaxic apparatus with ear, eye and bite bars. Pupils were maximally dilated with atropine (1%), and appropriate contact lenses were used to protect the corneas. Neosynephrine (5%) was administered to retract the nictitating membranes. Glucose (5%)-saline (0.9%) solution containing a mixture of urethane (20 mg/hr/kg body weight) and gallamine triethiodide (10 mg/hr/kg body weight) was infused intravenously to keep the animal anesthetized and paralysed. Expired pCO_2 was maintained at approximately 3.8%.

The level of anaesthesia was closely assessed throughout the experiment by continuously monitoring the animal's heart rate (about 180−220 pulses/min) and ECG to ensure that the animals were not responding to pain. The skull and dura over V1 (area 17) were removed with a fine surgery under light microscope. Single-unit recordings were performed using a glass-coated tungsten microelectrode (with an impedance of 3−5 MΩ) which was driven by a hydraulic micromanipulator (Narishige, Japan). The small hole over V1 was filled with 4% agar solution in saline and sealed with wax. After the preparation was complete, the optic discs of the two eyes were reflected onto a movable transparent tangent screen positioned 57 cm from the retina and overlapped with the CRT monitor used for stimulus presentation. The area centralis of each eye was located prior to physiological recording based on the position of the optic discs reflected onto the tangent screen (Bishop et al, 1962).

Visual stimuli

Visual stimuli were drifting sinusoidal gratings shown on a CRT monitor (resolution 1 024×768, refresh rate 85 Hz) positioned 57 cm from the animal's eyes. The program to generate the stimuli was written in MATLAB, using the extensions provided by the high-level Psychophysics Toolbox (Brainard, 1997) and low-level VideoToolbox (Pelli, 1997). Once a single unit was isolated, the cell's receptive field center was carefully located by consecutively presenting a series of computer-generated light spots on the CRT. By comparing the neuron's response to a series of stimulus package, we determined the optimal stimulus orientation, motion direction, temporal and spatial frequency and stimulus size for each cell. Then, the cell's response to a prolonged (30 s) stimulation with optimal stimulus was

recorded, which was used to assess the neuronal response properties during adaptation. Each stimulus was presented monocularly to the dominant eye and repeated 4-6 times with a 3-minute interval between each trial for functional recovery of the recorded cell. Before each stimulus was presented, spontaneous activity was acquired during a 10 s period while a mean luminance was shown on the screen.

The contrast of each stimulus used was set at 100%. The mean luminance of the display was 19 cd/m^2, and the environmental ambient luminance on the cornea was 0.1 lux.

Data analysis

After the signal was amplified with a microelectrode amplifier (Nihon Kohden, Japan) and differential amplifier (Dagan 2400A, USA), action potentials were fed into a window discriminator with an audio monitor. The original voltage traces were digitized using an acquisition board (National Instruments, USA) controlled by IGOR (WaveMetrics, USA), and saved for later analysis. The response of a cell to a drifting sinusoidal grating was defined as the mean firing rate (spontaneous activity substracted) corresponding to the time of stimulus modulation, which was used to draw the orientation, temporal and spatial frequency tuning curves. Preferred orientation was calculated as previously described (Schmolesky et al, 2000; Hua et al, 2006; Hua et al, 2010). The optimal temporal and spatial frequency of each cell were determined respectively by comparing the cell's mean firing rate to high contrast (100%) grating stimuli with different temporal and spatial frequencies , and selecting the temporal and spatial frequency with the maximum response.

To determine if neurons included in this study exhibited distinct adaptation to visual stimulation, the adaptation index (AI) was calculated respectively from each cell's response to the prolonged optimal stimulus and defined as the mean firing (spontaneous activity substracted) of the cell's average response during the last 5 s of stimulus adaptation, a period when the neuron's response retained a stable minimum level, to the average response during the initial 5 s of adaptation (Figure 1A). The smaller the AI, the stronger the adaptation of the cell. Cells with adaptation index ≥1 were treated as showing no adaptation to visual stimulation and excluded from our data analysis.

Two or more adjacent spikes with ISI (interspikes interval) ⩽20 ms were classified as a burst. A:Voltage trace of a cell's response during absence (0-15 s) and presence (15-45 s) of visual stimulation. A spike above the broken horizontal line is counted as an action potential; B:Burst time stamp in the cell's response during the initial 5 s of adaptation. The mean BF (burst frequency), IBI (interbursts interval), BL (burst length),

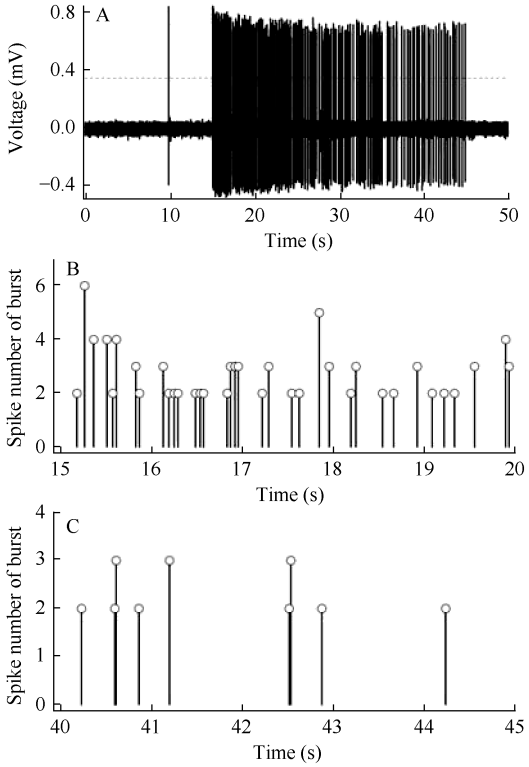

Figure 1 Burst detection from a cell's response to visual stimulation during the initial 5 s and the last 5 s of adaptation period respectively

BD (burst duration) and ISI (interspikes interval) was 7.2 burst/s, 0.135 s, 2.72 spikes/burst, 18.6 ms and 6.4 ms respectively; C:Burst time stamp in the cell's response to the last 5 s of stimulation. The mean BF, IBI, BL and ISI was 1.8 burst/s, 0.501 s, 2.33 spikes/burst, 26.8 ms and 12.9 ms respectively.

To disclose how visual adaptation influences burst firing of a cell's response, we compared burst firing properties of each cell's response at the initial 5 s and last 5 s of prolonged visual stimulation. We used a simple method to define bursts as strings of spikes with only two parameters: a minimum number of spikes per burst and a maximum interspike interval (ISI) (Turnbull et al, 2005). In this study, we set the minimum number of spikes per burst as 2, which was consistent with previous studies on the burst identification of visual cortical and subcortical neurons in cats (Mandl, 1993; DeBusk et al, 1997). According to the probability for two neighboring spikes to integrate (Traub & Miles, 1991; Barbieri et al, 2001), we combined both short and long ISI bursts (DeBusk et al, 1997) in data analysis and defined a maximum ISI as 20 ms. After the bursts have been identified, the mean burst frequency (BF: bursts/s), interbursts interval (IBI: interval between neighboring bursts), burst length (BL: spikes per burst), burst duration (BD: time interval from the first spike to the last

spike within a burst) and interspikes interval (ISI) within bursts were acquired (Figure 1B,C).

All values were expressed as mean±*SD*. Variations of BF, IBI, BL, BD and ISI in the neuronal response between different periods of adaptation were assessed using paired *t*-test or analysis of variance (ANOVA).

RESULTS

A total of 151 cells from 4 young adult cats were studied (Table 1), comprised of 65 simple cells and 86 complex cells. All cells had receptive fields within 8 degrees from the central area of the dominant eye. Measured from the mean firing rate of neuronal response, all studied cells showed an evident adaptation to prolonged visual stimulation (30 s), as indicated by the adaptation index ranged from 0.11-0.97. Because simple and complex cells showed no significant difference in adaptation index ($F(1,149)=0.298$, $P=0.586$), data from the two types of cells were combined for statistical analysis.

Table 1 Changes of burst firing properties of V1 neurons during adaptation to prolonged visual stimulation in four cats

	Cat1	Cat2	Cat3	Cat4
CN	26	56	34	35
AI	0.59±0.22	0.65±0.18	0.54±0.21	0.49±0.17
Burst firing during the initial 5s of adaptation				
BF	4.54±2.10	5.85±3.48	5.17±2.58	4.80±1.62
IBI	0.24±0.09	0.21±0.10	0.22±0.09	0.23±0.08
BL	4.86±0.69	5.30±0.88	5.14±0.79	5.09±0.97
BD	40.7±21.2	47.3±24.5	46.1±21.0	44.5±20.6
ISI	8.31±4.40	8.70±3.87	8.85±3.42	8.90±4.25
Burst firing during the last 5s of adaptation				
BF	2.85±1.62	3.85±2.07	2.95±1.62	2.34±1.16
IBI	0.41±0.29	0.31±0.16	0.47±0.50	0.48±0.35
BL	4.29±0.68	4.88±0.93	4.61±0.97	4.49±0.86
BD	53.6±16.3	55.1±25.0	59.1±19.8	53.8±20.5
ISI	12.5±3.36	11.3±4.66	13.1±4.17	12.2±4.57

CN and AI denote cell number and mean adaptation index of V1 cells in each cat.

BF, IBI, BL, BD and ISI represent the mean burst frequency (bursts/s), interbursts interval (s), burst length (spikes/burst), burst duration (ms) and interspikes interval (ms) of neuronal response in each cat.

Effects of adaptation on burst and isolated firing

To determine if burst firing and isolated firing of V1 cells were equally affected by adaptation, we compared the effects of adaptation on isolated spikes and burst spikes in the same neuron. Paired *t*-test showed that adaptation resulted in a significant reduction of both burst spikes and isolated spikes (all $P<0.0001$) (Figure 2A). The ratio of burst spikes to total spikes during the last 5 s of adaptation was significantly decreased as compared with that during the initial 5 s ($P<0.01$) (Figure 2B). However, the ratio of isolated spikes to total spikes during the last 5 s of adaptation was significantly increased when compared with that during the initial 5s ($P<0.01$) (Figure 2B). Therefore, adaptation of V1 neurons to prolonged visual stimulation decreased its burst firing more specifically than isolated firing.

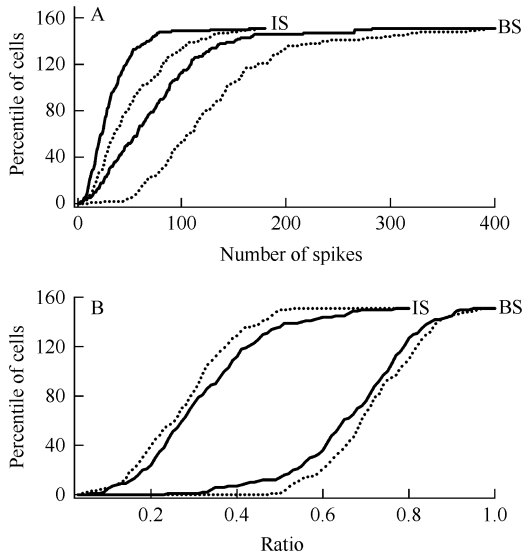

Figure 2 Effects of adaptation on burst spikes (BS) and isolated spikes (IS)

A: show the percentile distribution of cells with different range of spikes during the initial 5 s (dotted curves) versus the last 5 s of adaptation; B: show the percentile distribution of cells with different ratio of burst spikes or isolated spikes to total spikes during the initial 5 s (dotted curves) versus the last 5 s of adaptation.

Burst frequency and interbursts interval

To uncover how adaptation affected burst firing, we examined first the effects of adaptation on burst occurrence frequency (BF) of neuronal response by comparing the mean BF of V1 cells during the initial 5 s (15−20 s) and the last 5 s (40−45 s) of adaptation to prolonged visual stimulation. Most cells (64.2%) had a BF larger than or equal to 4 bursts/s during the initial 5 s of adaptation, whereas only a small part of cells (28.5%) had a BF larger than or equal to 4 bursts/s during the last 5 s of adaptation (Figure 3A). The mean BF of V1 cells during the last 5 s of adaptation to visual stimulation was significantly lower than that during the initial 5 s (paired *t*-test, $P<0.000001$). Therefore, adaptation to visual stimulation greatly decreased BF of V1 cells.

The interbursts interval (IBI) change of V1 cells during adaptation to prolonged visual stimulation was also examined. The majority of cells (81.5%) had an IBI shorter than 0.3 s during the initial 5 s of adaptation, whereas more than half of cells (57.6%) had an IBI equal to or longer than 0.3 s during the last 5 s of adaptation

(Figure 3B). The mean IBI value of V1 cells during the last 5 s of adaptation was significantly larger than that during the initial 5 s (paired *t*-test, $P<0.00001$).

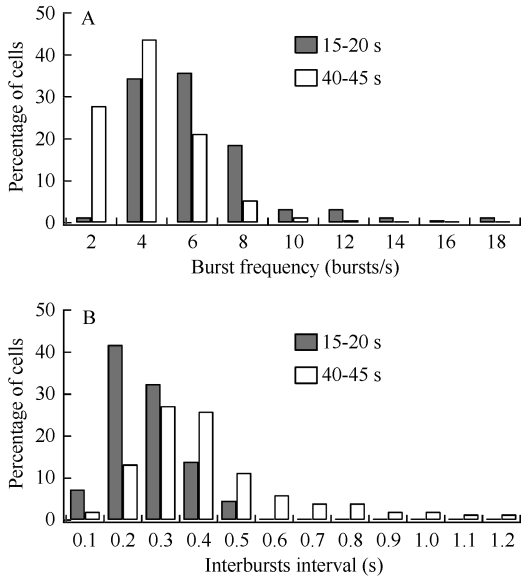

Figure 3 Percentage of cells with different range of burst frequency (A) and interbursts interval (B) during the initial 5 s and the last 5 s of adaptation to prolonged visual stimulation

Burst length, burst duration and interspikes interval

Previous studies showed that burst length (BL) is closely related to stimulus information encoding and synaptic transmission reliability (DeBusk et al, 1997). To examine how visual adaptation influences visual signal processing of visual cortical cells, we compared the BL of V1 neurons during the initial 5 s and the last 5 s of adaptation to visual stimulation. As indicated in Figure 4A, more than half of cells (55%) had a BL value equal to or larger than 6 spikes/burst during the initial 5 s of adaptation, while a smaller portion of cells (33.8%) had a BL value equal to or larger than 6 spikes/burst during the last 5 s of adaptation. Paired *t*-test showed that the mean BL of V1 neurons during the last 5 s of adaptation was significantly smaller than that during the initial 5 s of adaptation ($P<0.0001$). Accordingly, we concluded that visual adaptation decreased BL of neuronal response in V1.

A decreased BL in the neuronal response during adaptation could be caused by shortened burst duration (BD) or an increased interspikes interval (ISI) or both. To assess these possibilities, we compared the BD and ISI of V1 neurons during the initial 5 s and the last 5 s of adaptation to visual stimulation. Contrary to what we expected, the BD of V1 neurons actually increased during adaptation. Nearly half the cells (46%) exhibited a BD less than 60 ms during the initial 5 s of adaptation to visual stimulation, while most cells (72.8%) had a BD value equal to or larger than 60 ms during the last 5 s of adaptation (Figure 4B). The mean BD of V1 neurons during the last 5 s of visual adaptation (55.4±21.4 ms),significantly longer than that during the initial 5 s of adaptation (45.2±22.2 ms) (paired *t*-test, $P<0.0001$). Consistent with our expectations, however, the ISI of V1 neurons was significantly lengthened during adaptation to prolonged visual stimulation. The majority of cells (71.5%) displayed a mean ISI value smaller than 12 ms during the initial 5 s of adaptation, whereas most cells (61.6%) had a mean ISI equal to or larger than 12 ms during the last 5 s of adaptation (Figure 4C). The mean ISI value of V1 neurons during the last 5 s of adaptation (12.1±4.3 ms) was significantly greater than during the initial 5 s of adaptation (8.7±3.9 ms) (paired *t*-test, $P<0.000001$). Therefore, a reduced BL of V1 cells during visual adaptation was likely caused by an increased ISI within burst.

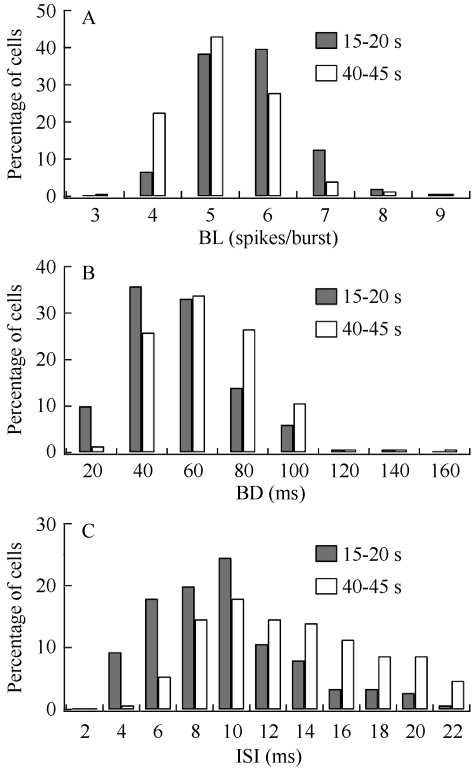

Figure 4 Percentage of cells with different range of BL (A), BD (B) and ISI (C) during the initial 5 s and the last 5 s of adaptation to prolonged visual stimulation

BL, BD and ISI represent burst length (spikes/burst), burst duration (ms) and interspikes interval (ms) within bursts respectively.

DISCUSSION

Adaptation mechanisms

Visual cortical neurons show a reduced firing rate to prolonged visual stimulation. The underlying neural basis for this, however, remains unresolved (Kohn, 2007; Hua et al, 2009). Based on analyses of the mean firing

rate of neuronal response, previous studies proposed several models to explain the adaptation phenomenon (Kohn, 2007). The contrast gain control mechanism (Carandini and Ferster, 1997; Sanchez-Vives et al, 2000), which suggested a strong somatic afterhyperpolarization due to an increased potassium ion current triggered by sodium ion influx during prolonged stimulation, cannot interpret the specificity of visual adaptation to the test stimulus. Excitatory synaptic depression can account for stimulus-specificity of adaptation; however, *in vivo* experiments lack convincing evidence to support this point of view (Chung et al, 2002; Nowak et al, 2005; Reig et al, 2006).

Inhibitory synaptic strengthening is another alternative mechanism that may underlie adaptation process. Nevertheless, *in vivo* electrophysiology research shows that manipulating local inhibition by the iontophoretic administration of GABA or $GABA_A$ receptor antagonist could not modify the extent of adaptation of visual cortical neurons to visual stimulation (DeBruyn & Bonds, 1986; Vidyasagar, 1990). Modeling studies proposed a network mechanism concerning a relative weight of recurrent excitation and inhibition in local circuitry (Teich & Qian, 2003; Compte & Wang, 2006), which may help clarify the above-mentioned discrepancy in the interpretation of adaptation. Unfortunately, no direct *in vivo* experimental evidence is available at present to elucidate this mechanism.

Burst firing, or spike train, neuronal responses contain both spike rate and spike timing information (Reich et al, 2000). For example, burst frequency (BF) and burst length (BL), which are linearly and nonlinearly proportional to the mean firing rate of neuronal response (DeBusk et al, 1997), can represent spike rate coding, whereas burst duration (BD) and the interspikes interval (ISI) within bursts can serve as determinants of spike timing (Dan et al, 1998; Usrey et al, 1998; Reich et al, 2000). Therefore, examining the burst firing properties of neurons during adaptation will provide an information in order to assess the changes in the neuronal signatures in the neural network (Snider et al, 1998). In this study, we found that both mean BD and ISI value of V1 neurons significantly increased during adaptation (Figure 4B,C), which indicates that neuronal activities from lateral or feedback connections might increase with adaptation. Additionally, we also found that the mean BF and BL of V1 neurons were significantly decreased during adaptation (Figure 3A, Figure 4A), suggesting that an inhibitory synaptic strengthening (DeBusk et al, 1997) may have also occurred. This finding was in direct contradiction to previous studies, which showed that manipulation of intracortical inhibition in adapted neurons had little effect on its adaptation strength (DeBruyn & Bonds, 1986; Vidyasagar, 1990). Likely, the decreased BF and BL of the adapted neuron are attributable to its presynaptic depression and/or postsynaptic somatic afterhyperpolarization. Based on polysynaptic connections between cortical pyramidal neurons and inhibitory interneurons (Szabadics et al, 2006; Ren et al, 2007; Silberberg & Markram, 2007; Silberberg, 2008), we propose that, due to a decreasing BF and BL, the adapted neuron might gradually inactivate its inhibitory driven interneurons, which could in turn trigger more excitatory inputs from neurons in the surroundings or higher visual cortical areas to the adapted neuron by lateral or feedback connections , and thus result in an increase of BD and ISI, similar to what we found in this study.

In conclusion, adaptation of V1 neurons to visual stimulation decreased BF and BL, probably by presynaptic depression and/or postsynaptic somatic afterhyperpolarization, and thus contributed to firing rate reduction, whereas the spike timing change of the adapted neuron, as indicated by an increase of BD and ISI, might be caused by an improved neuronal activities from lateral and/or feedback connections. Therefore, an interplay of neuronal activities within local network circuitry, as indicated by reduced activities from feedforward connections and increased activities from lateral and/or feedback connections, could underlie the adaptation of V1 neurons to prolonged visual stimulation. Further investigations with *in vivo* multielectrode array recording and patch clamping techniques are needed to explore this speculation more fully.

Biological implications of adaptation

Due to limited psychophysical data, it remains unclear whether adaptation improves the detectability or discriminability of adapted stimuli (Abbonizio et al, 2002; Greenlee & Heitger, 1988; Maattanen & Koenderink, 1991) or novel stimuli (Dragoi et al, 2002; Hosoya et al, 2005; Sharpee et al, 2006). According to current computational neuroscience research, burst firing in a neuron's response is more effective than single spikes in eliciting a time-related response in its driven neurons, and longer bursts are more effective than shorter ones (Snider et al, 1998; Krahe & Gabbiani, 2004). In this study, we found that adaptation caused a significant reduction in burst frequency (BF) and burst length (BL), which suggested that the information transmitted by V1 neurons regarding the adapted visual stimuli actually became less reliable during adaptation. Therefore, we propose that adaptation may exacerbate the detection of adapted stimuli, but may also improve the sensitivity of the visual system to novel stimuli in the field of vision. Further psychophysical experiments are needed to clarify this issue.

References

Abbonizio G, Langley K, Clifford CW. 2002. Contrast adaptation may enhance contrast discrimination. *Spatial Vision,* **16**(1): 45-58.

Baccus SA, Meister M. 2002. Fast and slow contrast adaptation in retinal circuitry. *Neuron,* **36**(5): 909-919.

Barbieri R, Quirk MC, Frank LM, Wilson MA, Brown EN. 2001. Construction and analysis of non-Poisson stimulus-response models of neural spiking activity. *Journal of Neuroscience Methods,* **105**(1): 25-37.

Bishop PO, Kozak W, Vakkur GJ. 1962. Some quantitative aspects of the cat's eye: axis and plane of reference, visual field co-ordinates and optics. *The Journal of Physiology,* **163**(3): 466-502.

Brainard DH. 1997. The psychophysics toolbox. *Spatial Vision,* **10**(4): 433-436.

Carandini M, Ferster D. 1997. A tonic hyperpolarization underlying contrast adaptation in cat visual cortex. *Science,* **276**(5314): 949-952.

Cattaneo A, Maffei L, Morrone C. 1981. Patterns in the discharge of simple and complex visual cortical cells. *Proceedings of the Royal Society-B Biological Sciences,* **212**(1188): 279-297.

Chung SY, Li XR, Nelson SB. 2002. Short-term depression at thalamocortical synapses contributes to rapid adaptation of cortical sensory responses *In Vivo*. *Neuron,* **34**(3): 437-446.

Compte A, Wang XJ. 2006. Tuning curve shift by attention modulation in cortical neurons: a computational study of its mechanisms. *Cerebral Cortex,* **16**(6): 761-778.

Dan Y, Alonso JM, Usrey WM, Reid RC. 1998. Coding of visual information by precisely correlated spikes in the lateral geniculate nucleus. *Nature Neuroscience,* **1**(6): 501-507.

DeBruyn EJ, Bonds AB. 1986. Contrast adaptation in cat visual cortex is not mediated by GABA. *Brain Research,* **383**(1-2): 339-342.

DeBusk BC, DeBruyn EJ, Snider RK, Kabara JF, Bonds AB. 1997. Stimulus-dependent modulation of spike burst length in cat striate cortical cells. *Journal of Neurophysiology,* **78**(1): 199-213.

Dragoi V, Sharma J, Miller EK, Sur M. 2002. Dynamics of neuronal sensitivity in visual cortex and local feature discrimination. *Nature Neuroscience,* **5**(9): 883-891.

Duong T, Freeman RD. 2007. Spatial frequency-specific contrast adaptation originates in the primary visual cortex. *Journal of Neurophysiology,* **98**(1): 187-195.

Eggermont JJ, Smith GM. 1996. Burst-firing sharpens frequency-tuning in primary auditory cortex. *Neuroreport,* **7**(3): 753-757.

Greenlee MW, Heitger F. 1988. The functional role of contrast adaptation. *Vision Research,* **28**(7): 791-797.

Hosoya T, Baccus SA, Meister M. 2005. Dynamic predictive coding by the retina. *Nature,* **436**(7047): 71-77.

Hua TM, Li GZ, Tang CC, Wang ZH, Chang S. 2009. Enhanced adaptation of visual cortical cells to visual stimulation in aged cats. *Neuroscience Letters,* **451**(1): 25-28.

Hua TM, Li XR, He LH, Zhou YF, Wang YC, Leventhal AG. 2006. Functional degradation of visual cortical cells in old cats. *Neurobiology of Aging,* **27**(1): 155-162.

Hua TM, Bao PL, Huang CB, Wang ZH, Xu JW, Zhou YF, Lu ZL. 2010. Perceptual learning improves contrast sensitivity of V1 neurons in cats. *Current Biology,* **20**(10): 887-894.

Kohn A. 2007. Visual adaptation: physiology, mechanisms, and functional benefits. *Journal of Neurophysiology,* **97**(5): 3155-3164.

Krahe R, Gabbiani F. 2004. Burst firing in sensory systems. *Nature Reviews Neuroscience,* **5**(1): 13-23.

Lisman JE. 1997. Bursts as a unit of neural information: making unreliable synapses reliable. *Trends in Neurosciences,* **20**(1): 38-43.

Maattanen LM, Koenderink JJ. 1991. Contrast adaptation and contrast gain control. *Experimental Brain Research,* **87**(1): 205-212.

Mandl G. 1993. Coding for stimulus velocity by temporal patterning of spike discharges in visual cells of cat superior colliculus. *Vision Research,* **33**(11): 1451-1475.

Nowak LG, Sanchez-Vives MV, McCormick DA. 2005. Role of synaptic and intrinsic membrane properties in short-term receptive field dynamics in cat area 17. *Journal of Neuroscience,* **25**(7): 1866-1880.

Oswald A-MM, Chacron MJ, Doiron B, Bastian J, Maler L. 2004. Parallel processing of sensory input by bursts and isolated spikes. *Journal of Neuroscience,* **24**(18): 4351-4362.

Pelli DG. 1997. The videotoolbox software for visual psychophysics: transforming numbers into movies. *Spatial Vision,* **10**(4): 437-442.

Reich DS, Mechler F, Purpura KP, Victor JD. 2000. Interspike intervals, receptive fields, and information encoding in primary visual cortex. *The Journal of Neuroscience,* **20**(5): 1964-1974.

Reig R, Gallego R, Nowak LG, Sanchez-Vives MV. 2006. Impact of cortical network activity on short-term synaptic depression. *Cerebral Cortex,* **16**(5): 688-695.

Ren M, Yoshimura Y, Takada N, Horibe S, Komatsu Y. 2007. Specialized inhibitory synaptic actions between nearby neocortical pyramidal neurons. *Science,* **316**(5825): 758-761.

Sanchez-Vives MV, Nowak LG, McCormick DA. 2000. Membrane mechanisms underlying contrast adaptation in cat area 17 *in vivo*. *The Journal Neuroscience,* **20**(11): 4267-4285.

Schmolesky MT, Wang Y, Pu M, Leventhal AG. 2000. Degradation of stimulus selectivity of visual cortical cells in senescent rhesus monkeys. *Nature Neuroscience,* **3**(4): 384-390.

Sharpee TO, Sugihara H, Kurgansky AV, Rebrik SP, Stryker MP, Miller KD. 2006. Adaptive filtering enhances information transmission in visual cortex. *Nature,* **439**(7079): 936-942.

Shou T, Li XR, Zhou YF, Hu B. 1996. Adaptation of visually evoked responses of relay cells in the dorsal lateral geniculate nucleus of the cat following prolonged exposure to drifting gratings. *Visual Neuroscience,* **13**(4): 605-613.

Silberberg G. 2008. Polysynaptic subcircuits in the neocortex: Spatial and temporal diversity. *Current Opinion in Neurobiology,* **18**(3): 332-337.

Silberberg G, Markram H. 2007. Disynaptic inhibition between neocortical pyramidal cells mediated by martinotti cells. *Neuron,* **53**(5): 735-746.

Smirnakis SM, Berry MJ, Warland DK, Bialek W, Meister M. 1997. Adaptation of retinal processing to image contrast and spatial scale. *Nature,* **386**(6620): 69-73.

Snider RK, Kabara JF, Roig BR, Bonds AB. 1998. Burst firing and modulation of functional connectivity in cat striate cortex. *Journal of Neurophysiology,* **80**(2): 730-744.

Szabadics J, Varga C, Molnar G, Olah S, Barzo P, Tamas G. 2006. Excitatory effect of GABAergic axo-axonic cells in cortical microcircuits. *Science,* **311**(5758): 233-235.

Teich AF, Qian N. 2003. V1 orientation plasticity is explained by broadly tuned feedforward inputs and intracortical sharpening. *Visual Neuroscience,* **27**(1-2): 57-73.

Thomson AM, Deuchars J. 1997. Synaptic interactions in neocortical local circuits: dual intracellular recordings *in vitro*. *Cerebral Cortex,* **7**(6): 510-522.

Traub RD, Miles R. 1991. Multiple modes of neuronal population activity emerge after modifying specific synapses in a model of the CA3 region of the hippocampus. *Annals of the New York Academy of Sciences,* **627**: 277-290.

Turnbull L, Dian E, Gross G. 2005. The string method of burst identification in neuronal spike trains. *Journal of Neurosciences Methods,* **145**(1-2): 23-35.

Usrey WM, Reppas JB, Reid RC. 1998. Paired-spike interactions and synaptic efficacy of retinal inputs to the thalamus. *Nature,* **395**(6700): 384-387.

Vidyasagar TR. 1990. Pattern adaptation in cat visual cortex is a co-operative phenomenon. *Neuroscience,* **36**(1): 175-179.

科学出版社生物分社 2013 年 3、4 月书讯

分子生物学（第五版）

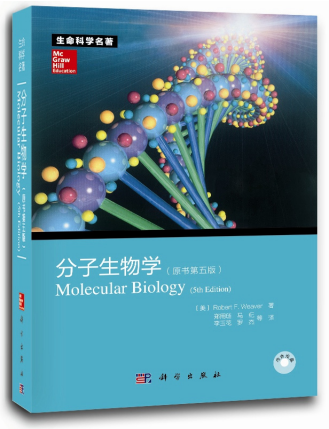

作者：(美)Robert F. Weaver 著
ISBN：9787030368539
定价：160
开本：16　**装帧：**平装　**页码：** 944
初版时间：3/1/2013
专业分类：01Q-3075·0101
读者对象：《分子生物学（第五版）》中理论讲述逻辑严密，实验过程提炼清晰，特色鲜明、内容详尽，图文并茂，易读易记，是一本生命科学相关专业的研究生，以及从事该方面科研、教学工作的人员不可多得的优秀参考书。

内容介绍

分子生物学是生命科学发展过程中诞生的一门实验性极强的新兴学科。美国著名分子生物学家 Robert F.Weaver 遵循这一学科发展的特点，于 1999 年出版了 Molecular Biology 一书。《分子生物学（第五版）》以原始研究论文为基础，通过对实验的设计、对结果的分析而逐步展开对分子生物学理论的讲述，文字通俗流畅，叙述由浅入深。随着学科的迅速发展，几经修订再版的《分子生物学》第五版共有导论，分子生物学方法，原核生物的转录，真核生物的转录，转录后加工，翻译，DNA 复制、重组和转座，以及基因组等 8 个部分共 25 章的内容，书后还附有术语表。每一章节都以提出科学问题、展开研究过程开始，以提供思考习题、推荐阅读文献结束。

作译者介绍

Rob Weaver 出生于美国堪萨斯州的首府托皮卡市，在弗吉尼亚州的阿灵顿地区长大。1964 年在俄亥俄州的乌斯勒学院获得化学学士学位。1969 年在杜克大学获得生物化学专业博士学位，此后他在加州大学旧金山分校从事了两年的博士后研究工作，师从 Willam J.Rutter 教授研究真核生物 RNA 聚合酶的结构。

1971 年他受聘于堪萨斯大学，任生物化学助理教授，后晋升为副教授，并于 1981 年任教授。自 1984 年以来，Rob Weaver 一直担任生物化学系的系主任，1995 年开始担任文理学院副院长。

文理学院管辖 14 个不同的系和研究中心，Weaver 教授分管科学和数学系。作为一位分子生物学教授，他主讲分子生物学概论和癌症分子生物学两门课程，并指导本科生和研究生在实验室进行感染鳞翅目幼虫的杆状病毒分子生物学方面的研究工作。

Weaver 教授的研究受到美国国立卫生研究所、美国国家科学基金和美国癌症协会的资助，发表了多篇科学论文。并且他还与同事一道合著了两本遗传学教科书，为《美国国家地理杂志》撰写过两篇分子生物学方面的文章。作为美国癌症协会的研究人员，他在欧洲的两个实验室（瑞士的苏黎世和英国的牛津大学）分别进行了一年的访问研究。

本书特色or编辑荐语

Robert F. Weaver 的《分子生物学》一书历经十余年，已更新到第五版。最新版本秉承了本书的优良传统，特色鲜明、内容详尽，图文并茂，易读易记。最突出的特点是本书极富逻辑性，编写人性化，每个结论都由具体实验得出，这不但让读者记住了实验方法，更可以感受到分子生物学的精妙与美。此中文版排版清晰、美观，并赠送包含原版彩图的光盘。《分子生物学》第五版将是分子生物学领域最好的参考书。

动物学研究
DONGWUXUE YANJIU

Bimonthly, Since 1980
Volume 34 Issue E3 June 2013

ZOOLOGICAL RESEARCH EDITORIAL BOARD

Edited by Editorial Office of Zoological Research
(Kunming Institute of Zoology, the Chinese Academy of Sciences, 32 Jiaochang Donglu, Kunming, Yunnan, Post Code: 650223 Tel: +86 871 65199026 Fax: +86 871 65113532
E-mail: zoores@mail.kiz.ac.cn Website: http://www.zoores.ac.cn)

Editor-in-Chief: Yong-Gang YAO

Sponsored by Kunming Institute of Zoology, the Chinese Academy of Sciences; China Zoological Society©

Published by Science Press (16 Donghuangchenggen Beijie, Beijing 100717, China)

Printed by Kunming Xiaosong Plate Making & Printing Co, Ltd

Domestic distribution by Yunnan Post and all local post offices in China

International distribution by China International Book Trading Corporation (Guoji Shudian) P.O.BOX 399, Beijing 100044, China

ISSN 0254-2853/CN 53-1040/Q

Price: 7.00 USD/40.00 CNY Post No: BM358